NAVAL POSTGRADUATE SCHOOL

Monterey, California

THESIS

ESTIMATING MESOSCALE, OROGRAPHICALLY ENHANCED PRECIPITATION USING SYNOPTIC SCALE DATA

by

Michael D. Angove

December, 1991

Thesis Advisor: Dr. Wendell A. Nuss

DISCLAIMER NOTICE

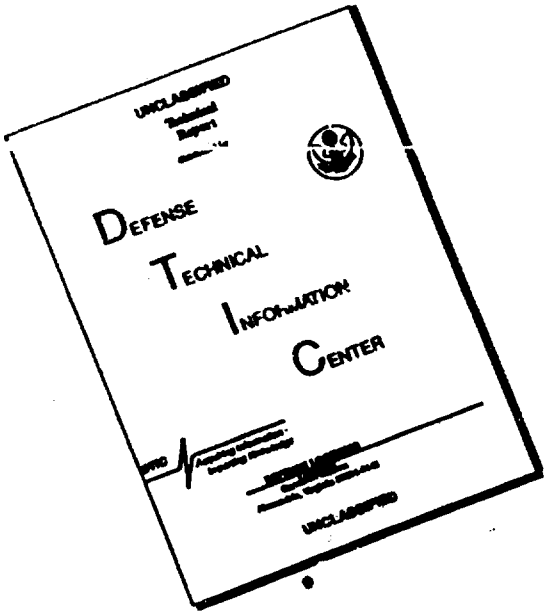

THIS DOCUMENT IS BEST QUALITY AVAILABLE. THE COPY FURNISHED TO DTIC CONTAINED A SIGNIFICANT NUMBER OF PAGES WHICH DO NOT REPRODUCE LEGIBLY.

REPORT DOCUMENTATION PAGE

1a REPORT SECURITY CLASSIFICATION UNCLASSIFIED	1b RESTRICTIVE MARKINGS
2a SECURITY CLASSIFICATION AUTHORITY	3 DISTRIBUTION/AVAILABILITY OF REPORT Approved for public release; distribution is unlimited.
2b DECLASSIFICATION/DOWNGRADING SCHEDULE	
4 PERFORMING ORGANIZATION REPORT NUMBER(S)	5 MONITORING ORGANIZATION REPORT NUMBER(S)
6a NAME OF PERFORMING ORGANIZATION Naval Postgraduate School 6b OFFICE SYMBOL (*If applicable*) 55	7a NAME OF MONITORING ORGANIZATION Naval Postgraduate School
6c ADDRESS (*City, State, and ZIP Code*) Monterey, CA 93943-5000	7b ADDRESS (*City, State, and ZIP Code*) Monterey, CA 93943-5000
8a NAME OF FUNDING/SPONSORING ORGANIZATION 8b OFFICE SYMBOL (*If applicable*)	9 PROCUREMENT INSTRUMENT IDENTIFICATION NUMBER
8c ADDRESS (*City, State, and ZIP Code*)	10 SOURCE OF FUNDING NUMBERS Program Element No / Project No / Task No / Work Unit Accession Number

11 TITLE (*Include Security Classification*)
ESTIMATING MESOSCALE, OROGRAPHICALLY ENHANCED PRECIPITATION USING SYNOPTIC SCALE DATA

12 PERSONAL AUTHOR(S) Angove, Michael, D.

13a TYPE OF REPORT	13b TIME COVERED	14 DATE OF REPORT (*year, month, day*)	15 PAGE COUNT
Master's Thesis	From To	December 1991	84

16 SUPPLEMENTARY NOTATION
The views expressed in this thesis are those of the author and do not reflect the official policy or position of the Department of Defense or the U.S. Government.

17 COSATI CODES			18 SUBJECT TERMS (*continue on reverse if necessary and identify by block number*)
FIELD	GROUP	SUBGROUP	Mesoscale orographically enhanced

19 ABSTRACT (*continue on reverse if necessary and identify by block number*)

A method for resolving the mesoscale distribution of precipitation over mountainous regions is developed using synoptic scale analyses and a 40 km resolution of topography. The method consists of calculating the saturated moisture flux at a level assumed to be the cloud base and correlating this quantity with observed precipitation. General correlation coefficients ranged from -0.2 under conditions poorly represented by the synoptic surface analysis to -0.55 when these analyses are more representative of actual forcing. When applied regionally, correlation improved dramatically, suggesting potential incorporation into precipitation forecasts over mountainous areas. Over wider regions of less defined topography correlation is weaker, but is still an improvement over the current synoptic scale precipitation forecast products.

20 DISTRIBUTION/AVAILABILITY OF ABSTRACT ☒ UNCLASSIFIED/UNLIMITED ☐ SAME AS REPORT ☐ DTIC USERS	21 ABSTRACT SECURITY CLASSIFICATION UNCLASSIFIED	
22a NAME OF RESPONSIBLE INDIVIDUAL Dr. Wendell A. Nuss	22b TELEPHONE (*Include Area code*) (408) 646-2308	22c OFFICE SYMBOL MRNU

DD FORM 1473, 84 MAR 83 APR edition may be used until exhausted
All other editions are obsolete

Approved for public release; distribution is unlimited.

ESTIMATING MESOSCALE, OROGRAPHICALLY ENHANCED PRECIPITATION USING SYNOPTIC SCALE DATA

by

Michael D. Angove
Lieutenant, United States Navy
B.S., Eastern Washington University, 1985

Submitted in partial fulfillment
of the requirements for the degree of

MASTER OF SCIENCE IN METEROROLOGY AND PHYSICAL OCEANOGRAPHY

from the

NAVAL POSTGRADUATE SCHOOL
December 1991

Author: _____
Michael D. Angove

Approved by: _____
Dr. Wendell A. Nuss, Thesis Advisor

_____
Dr. Patricia M. Pauley, Second Reader

_____
Dr. Robert L. Haney, Chairman
Department of Meteorology

ABSTRACT

A method for resolving the mesoscale distribution of precipitation over mountainous regions is developed using synoptic-scale analyses and topography with a 40 km resolution. The method consists of calculating the saturated moisture flux at a level assumed to be the cloud base and correlating this quantity with observed precipitation. General correlation coefficients ranged from -0.2 under conditions poorly represented by the synoptic surface analysis to -0.55 when these analyses are more representative of actual forcing. When applied regionally, correlation improved dramatically, suggesting potential incorporation into precipitation forecasts over mountainous areas. Over wider regions of less defined topography, correlation is weaker but is still an improvement over the current synoptic-scale precipitation forecast products.

TABLE OF CONTENTS

I. INTRODUCTION 1

II. BACKGROUND 4

III. PROCEDURE 7

A. THEORY 7

B. DERIVATION OF PRECIPITATION PARAMETER 8

C. DATA 13

IV. SYNOPTIC ANALYSIS 18

A. OVERVIEW 18

B. CYCLONE CHARACTERISTICS 22

1. 0000 UTC 28 February 1991 - 1200 UTC 02 March 1991 22

2. 1200 UTC 02 March 1991 - 1200 UTC 04 March 1991 25

3. Summary 27

V. RESULTS 28

A. OVERALL 28

1. Statistics 28

2. *Wqf* Distribution 31

a. 0000 UTC 28 February 1991 - 1200 UTC 02 March 1991 . . 31

b. 1200 UTC 02 March 1991 - 1200 04 March 1991 33

3. Correlation Limiting Factors 35

a. Synoptic Conditions 35

b. Smoothing 35

c. Location 38

d. Other Considerations 38

B. REGIONAL 45

1. Approach 45

2. Topographic Subregions 46

a. San Bernardino/San Gabriel 46

b. Santa Barbara 50

c. Southern Sierra Nevada 55

d. Northern Sierra Nevada 58

e. Shasta/Siskiyou 60

f. Non-mountainous Regions 65

3. Comparison to NGM Precipitation Forecasts 66

VI. CONCLUSIONS 68

A. APPLICATION TO FORECASTING 68

B. RECOMMENDATIONS 69

LIST OF REFERENCES 71

BIBLIOGRAPHY 73

INITIAL DISTRIBUTION LIST 74

ACKNOWLEDGEMENTS

This thesis is dedicated to my wife, Faith. It truly would not have been possible without her technical and moral support. I would also like to thank Professor Wendell Nuss for his uncommon willingness to help me understand the science of Meteorology. Also, thanks to Professor Patricia Pauley and Professor Robert Haney for their critical reviews of this thesis.

I. INTRODUCTION

The enhancement of synoptic-scale precipitation by topography is well understood, and has been routinely verified. Fine-mesh mesoscale models have proven particularly accurate in reflecting orographic influences on large-scale precipitation events (Colton 1976, Collier 1975). Simpler estimates of this enhancement factor have been shown to be almost exclusively functions of regional topography combined with low-level wind fields, synoptic-scale vertical motion, and a knowledge of the low-level relative humidity (Browning *et al.* 1975, Hill *et al.* 1981).

Thus far, only detailed mesoscale models have been able to reproduce the small-scale orographic enhancement process. With synoptic-scale precipitation products showing little or no regional structure, and mesoscale forcing fields generally unavailable, forecasters rely mostly on local knowledge and vague statistical multipliers to predict areas of heavy rainfall. Consequently, the ability to quantify local orographic effects and their associated distribution of precipitation based solely on synoptically derived wind and moisture fields would be of particular use to the forecaster.

In this study, the above mentioned quantities of subsynoptic-scale topography and synoptic-scale wind and moisture data are combined in an effort to reproduce areas of enhanced precipitation during a series of eastern Pacific extratropical cyclones which passed over California during the period 1200 UTC 27 February 1991 to 1200 UTC 04 March 1991. Topography, combined with wind and moisture fields given by the

National Meteorological Center's (NMC) final analyses, produces a distribution of the total vertical moisture flux. This vertical moisture flux estimate is correlated with hourly precipitation data collected by the National Oceanic and Atmospheric Administration (NOAA), covering 244 reporting stations throughout California for the same period, to produce an equivalent rainfall amount.

The overall intent of this study is to aid forecasters in identifying areas most likely to experience orographic enhancement of precipitation for a given synoptic event and provide a quantitative precipitation estimate. This procedure may be of use in estimating seasonal snowpack levels in otherwise inaccessible regions, as well as providing near term flood potential for specific drainage basins, while only requiring synoptic-scale information. More specific objectives of this study are to:

- Assess the degree of accuracy to which precipitation distribution can be represented using mesoscale topography and large-scale wind and moisture fields.
- Develop a simple quantity, calculated locally from model output products, to represent the enhancement of precipitation due to topography.
- Present specific synoptic-scale conditions and/or regional topographic characteristics which either promote or discourage the use of this parameter.
- Determine the level of improvement, if any, the employment of this parameter shows over current precipitation forecast products.

Following a discussion of background work done in the field of orographic precipitation enhancement, an outline of the dynamical basis for the vertical moisture flux as a precipitation parameter is presented, [illegible] of the required input fields. Next, this parameter is correlated with observed precipitation to obtain a

statistical fit assigning specific precipitation accumulations to the calculated values followed by an examination of the factors which affect correlation. Results obtained by applying the precipitation parameter both generally and regionally are examined, including a comparison to current precipitation forecast aids (specifically, the Nested Grid Model (NGM) 12 hour precipitation forecast). Conclusions focus on the usefulness of this technique as a forecast aid.

II. BACKGROUND

It is certainly no secret that mountainous areas often receive greater amounts of precipitation than do upwind or downwind low-lying regions. However, it was not until Bergeron (1965) introduced his "seeder cloud - feeder cloud" concept that a specific mechanism for topographically enhanced precipitation became accepted. As described by Raddatz and Khandekar (1979) this process consists of low-level (feeder) clouds forming in upslope areas which "wash out" when seeded by raindrops falling from synoptic-scale (seeder) clouds above. The idea is that the feeder cloud is constantly replenished and will continue to enhance precipitation in proportion to its depth, provided seeding from above is uninterrupted. Storebo (1976) and Bader and Roach (1977) were able to confirm Bergeron's theories by results which related a 10% increase in precipitation to a 1000 m feeder cloud depth. Interestingly, Browning *et al.* (1974) suggested that in some instances (namely, cases of mid-level potential instability), orography alone could be responsible for generating precipitation, even if synoptic-scale seeding was not available. According to Browning *et al.* (1975), condensation over mountainous regions is roughly proportional to the low-level wind velocity component normal to the topographic barrier combined with synoptic-scale vertical motion and moisture quantities. This relationship was generally verified by the mesoscale numerical model developed by Collier (1975).

As mentioned in the introduction, Colton (1976) achieved remarkably accurate results using a fine-mesh (1.3 km grid) model [illegible] (1975), applied

to the Sierra Nevada of California. A key assumption made by Colton was to define the orographic precipitation as a quantity dependent on the presence of synoptic-scale precipitation. As such, his scheme is only able to enhance synoptic-scale precipitation, and cannot force precipitation based solely on orography.

A later study by Hill *et al.* (1981) further confirmed the seeder-feeder enhancement theory. They additionally showed that if the total precipitation rate exceeded a given threshold value (0.5 mm hr^{-1}), the topographic enhancement factor was not dependent on the background precipitation rate. In short, as long as the background rainfall rate was sufficiently high, enhancement was simply proportional to the low-level moist flow interacting with topography, and was not a function of the amount of seeding from above. This carries the important implication that orographically induced precipitation can simply be added to synoptic-scale rainfall to obtain a total, rather than the orographic term being a function of the synoptic-scale term. This relationship provides the basis for deriving the precipitation parameter described in the following chapter.

More recent studies have attempted to modify feeder-seeder theory to account for additional effects including stratification and wind drift. While showing the effect of stratification to be negligible as it relates to total washout, Carruthers and Choularton (1983) did show wind drift effects, which were not accounted for in models such as Bader and Roach (1977), to be detrimental to both local maxima and total enhancement by "advecting" orographic precipitation to downwind locations. Additionally, this study backed up the idea presented by Hill *et al.* (1981) that the enhancement is independent of seeding rate (also contradictory to the Bader and Roach (1977) model).

Most recently, Stow, Bradley and Gray (1991) conducted a study with results largely consistent with seeder-feeder theories, and emphasized the significant differences between the previous enhancement studies. They regarded the work so far conducted as inconsistent in terms of dealing with the effects of the low-level wind speed, seeding rate, and barrier height. Moreover, they felt that although the basic physics of topographic enhancement are well understood, refinement is required to handle the above inconsistencies. The present study is not concerned with any of these "refinements", but rather with using the existing theory to derive a simplified method of representing mesoscale-resolution topographically enhanced precipitation from exclusively synoptic-scale data.

It should be noted that topography plays a larger role in weather than simply enhancement of precipitation. In fact it has been shown that topography can influence the low- to mid-level flow in such a manner as to completely reposition large-scale pressure centers (Sawyer 1959), as well as greatly altering the small-scale wind patterns (Danard 1977). An attempt to combine small-scale deformation of the wind field due to topography with established enhancement theory was undertaken by Anderson and Nilsson (1990) and had only moderate success, mostly owing to large errors in obtaining precipitation measurements in drifting snow. Any deformation of the wind field by topography will be ignored in this thesis, in terms of calculating our precipitation parameter. As such, a main objective of this study is to determine the feasibility of representing mesoscale precipitation distributions solely on the basis of the actual mesoscale wind fields.

III PROCEDURE

A. THEORY

Preceding studies have estimated orographic enhancement of precipitation by determining the vertical extent of a feeder cloud which forms in upslope regions based on low-level winds and wet bulb potential temperature. This cloud depth can be directly related to orographically induced precipitation provided seeding from above (synoptic-scale rain) is available. Assuming the "washout" efficiency is properly handled, numerical models can easily determine the enhancement factor based on calculated feeder cloud depth (Raddatz and Khandekar 1979, Bader and Roach 1977).

Since the purpose of this study is to provide an easily-calculable means of estimating topographical enhancement of precipitation, a slightly different approach than a numerical model simulation is taken. This estimate of topographic precipitation enhancement is based on a "ground-up" quantity reflecting the total saturated moisture flux at a given height (assumed to be the cloud base), $(wq)_H$. Conceptual restraints are imposed such that any upward saturated moisture flux at this level is condensed, and not allowed to either be redistributed into higher levels of the atmosphere, or result in supersaturation. Essentially, any such flux is completely "washed-out" as precipitation. Since this flux is representative of precipitation only under saturated conditions, a threshold 700 mb relative humidity value of [illegible] relative humidity is used to represent saturation at the synoptic scale) will be applied to the $(wq)_H$ field.

B. DERIVATION OF PRECIPITATION PARAMETER

Bader and Roach (1977) used the following form of the continuity equation to represent the liquid water content:

$$\frac{Dq_L}{Dt} = C - A, \tag{1}$$

where Dq_L/Dt represents rate of change of liquid water content following the air parcel trajectory. C is used to represent the condensation rate while A is the rate of washout from above. It follows that Dq_v/Dt is simply the total precipitation minus evaporation under saturated conditions, such that

$$\frac{Dq_v}{Dt} = -(P - E), \tag{2}$$

where P and E stand for precipitation and evaporation, respectively. Following Holton (1979, pp 40-44),

$$\frac{dq_v}{dt} = \frac{\partial q_v}{\partial t} + \left(u\frac{\partial q_v}{\partial x} + v\frac{\partial q_v}{\partial y} + \omega\frac{\partial q_v}{\partial p} \right)$$

represents the total time derivative of q_v in terms of the local tendency and advective components. Rearrangement in vector notation and use of the isobaric form of the continuity equation with (2), gives

$$\frac{\partial q_v}{\partial t} + \nabla \cdot (q_v \vec{U}) = -(P - E). \tag{3}$$

Changes in the saturation specific humidity (q_v) result from temperature and pressure changes, which are largest due to vertical advection. Thus, the local tendency $\partial q_v / \partial t$ is smaller than the flux divergence $\nabla \cdot q\vec{U}$ and will be ignored in this calculation. The P-E term is the net condensation, which is equivalent to the rainfall when integrated over the depth of the atmosphere. The net condensation is written simply $\bar{P}$ in the following equations. We are left with

$$-\bar{P} = \nabla \cdot (q\vec{U}), \tag{4}$$

as a first-order approximation to the net precipitation. Separating (4) into horizontal and vertical components yields

$$-\bar{P} = \left[\frac{\partial (qu)}{\partial x} + \frac{\partial (qv)}{\partial y} \right] + \frac{\partial (q\omega)}{\partial p}.$$

This can be integrated from the surface to the top of the atmosphere H, to give

$$-\int_{P_0}^{P_H}\bar{P}dp+(q\omega)_{P_H}=(q\omega)_{P_0}+\int_{P_0}^{P_H}\left[\frac{\partial(qu)}{\partial x}+\frac{\partial(qv)}{\partial y}\right]dp. \tag{5}$$

where $(q\omega)_{P_H}$ represents total moisture flux at H, which is zero. The term $-\int_{P_0}^{P_H}\bar{P}dp$ represents the rainfall, R, and the right-hand side of equation (5) gives the contribution from both topographic uplift, $(q\omega)_{P_0}$, and synoptic-scale forcing, $+\int_{P_0}^{P_H}[\nabla_h\cdot(q\vec{U})]dp$. The synoptic-scale forcing is simply the net horizontal flux divergence of saturated air into the column. Because q_s is largest at low levels, the net moisture flux is dominated by the lower part of the atmosphere. Consequently, this term is approximated by the integrated moisture flux convergence from the surface to 700 mb. The approximate rainfall is then given by

$$R=(q\omega)_{P_0}+\int_{P_0}^{700}\left[\nabla_h\cdot(q\vec{U})\right]dp,$$

with R representing net precipitation in the column. Both terms appearing on the right-hand side of the equation are easily obtained from standard wind and moisture data

combined with surface topography. The 40 km resolution topography used in this study is shown in Figure 1. Specifically, the term $(q\omega)_{P_0}$ is given as $q_{P_0}[u\frac{\partial h}{\partial x}+v\frac{\partial h}{\partial y}]$, with u, v and h representing horizontal wind velocity components and surface slope, respectively, while q_{P_0} refers to the surface moisture value.

The surface forcing $(qw)_{P_0}$, and ultimately $(q\omega)_{P_0}$, was calculated using the 1000 mb wind field and topography in meters, with the 1000 mb winds treated as crudely representative of synoptic-scale surface winds for this purpose. The resultant surface-forced moisture flux is in units of $g/kg \cdot cm/s$. An approximate conversion to pressure coordinates is made by applying the relation $qw=-\rho g\omega q$.

The synoptic scale term $(-\int_{P_0}^{700}[\nabla\cdot(q\vec{U})]dp)$, is calculated using a centered finite difference scheme to compute the moisture flux divergence at levels specified by the wind and moisture field inputs. Summations over the desired vertical distance yield the net moisture flux divergence in the surface to 700 mb layer, which is the vertical moisture flux $q\omega$ through the 700 mb level. This is the quantity *w0f*, referred to in the Results chapter. Figures 2 and 3 show sample contoured surface vertical velocity and $q\omega$ flux fields obtained from these methods. The topography [illegible] in Figure 1 has been subjected to a five passes through a three point smoothing [illegible] to ensure this

quantity is of the same order of magnitude as the synoptically derived forcing in Figure 3. Finally, the total moisture flux at 700 mb, $(q\omega)_{700}$ (hereafter referred to as *wqf*), is obtained by simply adding the topographic and synoptic-scale components, utilizing the rough equivalency of $\mu bars^{-1}$ and cms^{-1} as described above (Figure 4). Thus both *w0f* and *wqf* are in units of $gkg^{-1}\mu bars^{-1}$. This unit definition applies to all figures showing *w0f* or *wqf* fields unless otherwise noted.

Note that this $(q\omega)_{700}$ quantity is <u>not</u> in units of rainfall. The actual associated rainfall is obtained by first employing a 75% 700 mb relative humidity threshold to the $(\omega q)_{700}$ field to ensure saturation. This field is then correlated with observed 12 hour accumulated precipitation centered on the analysis time. A linear regression is calculated, yielding a conversion factor based on the slope and y-intercept, allowing $(\omega q)_{700}$ quantities to represent 12 hour precipitation totals. For the overall correlation, no objective limitations are imposed other than the relative humidity threshold. Regional constraints are imposed, however, when examining the effectiveness of this technique in more localized mountainous regions.

Perhaps the most obvious limitation of using this quantity to estimate precipitation is its exclusion of sub-grid scale (i.e., convective) precipitation processes. While no effort is made to quantify the effect of topography on such precipitation, these conditions are identified using satellite imagery, and are noted as appropriate in the analysis and results section.

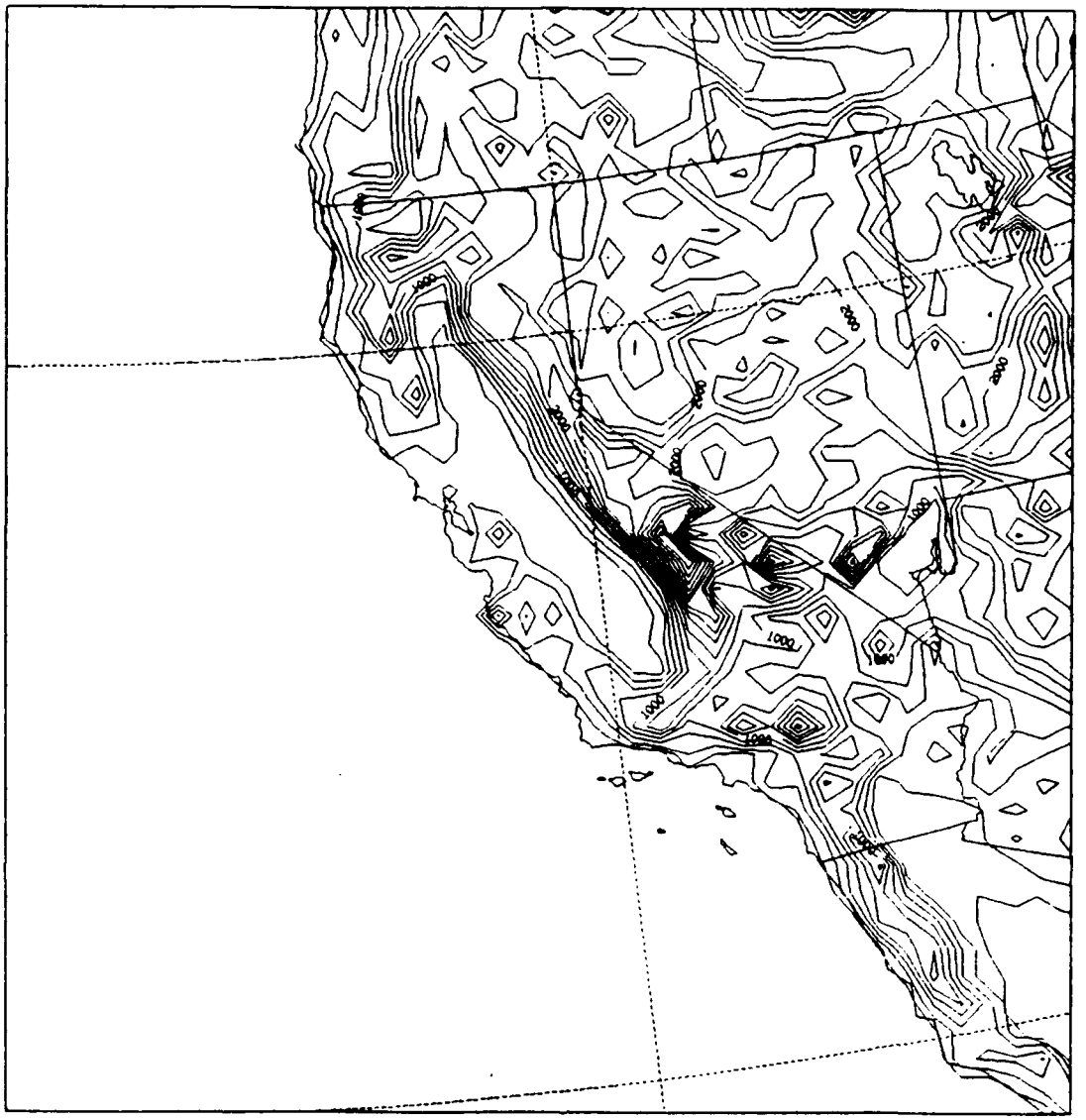

Figure 1. Topography (40 km resolution, in meters)

C. DATA

The saturated moisture flux quantity used to represent precipitation is calculated from NMC final Global Data Assimilation System (GDAS) analysis fields, which were then statistically fitted to hourly precipitation observations collected by NOAA. The

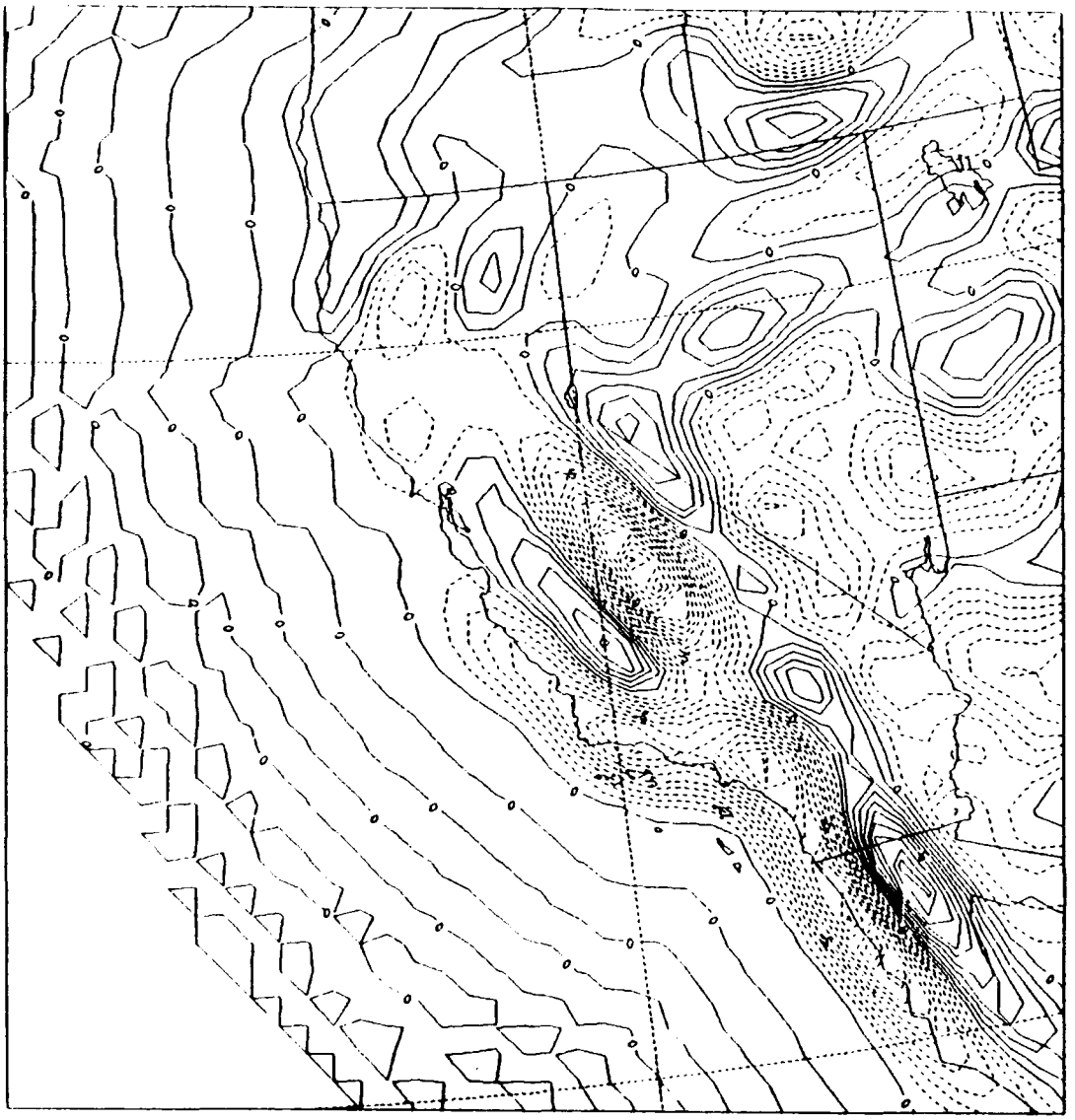

Figure 2. Smoothed orographically forced surface vertical velocity (cm/s). 1200 UTC 01 March 1991. Negative values correspond with upward velocities.

NMC GDAS analyses include twelve pressure levels from 1000 to 50 mb (as described by Kanamitsu 1989). For this study, the 2.5° NMC GDAS grid is interpolated to the 40 km grid on which the regional topography was derived. The wind and moisture fields at the 1000, 850 and 700 mb levels were used to calculate the vertically integrated moisture flux, *wqf*.

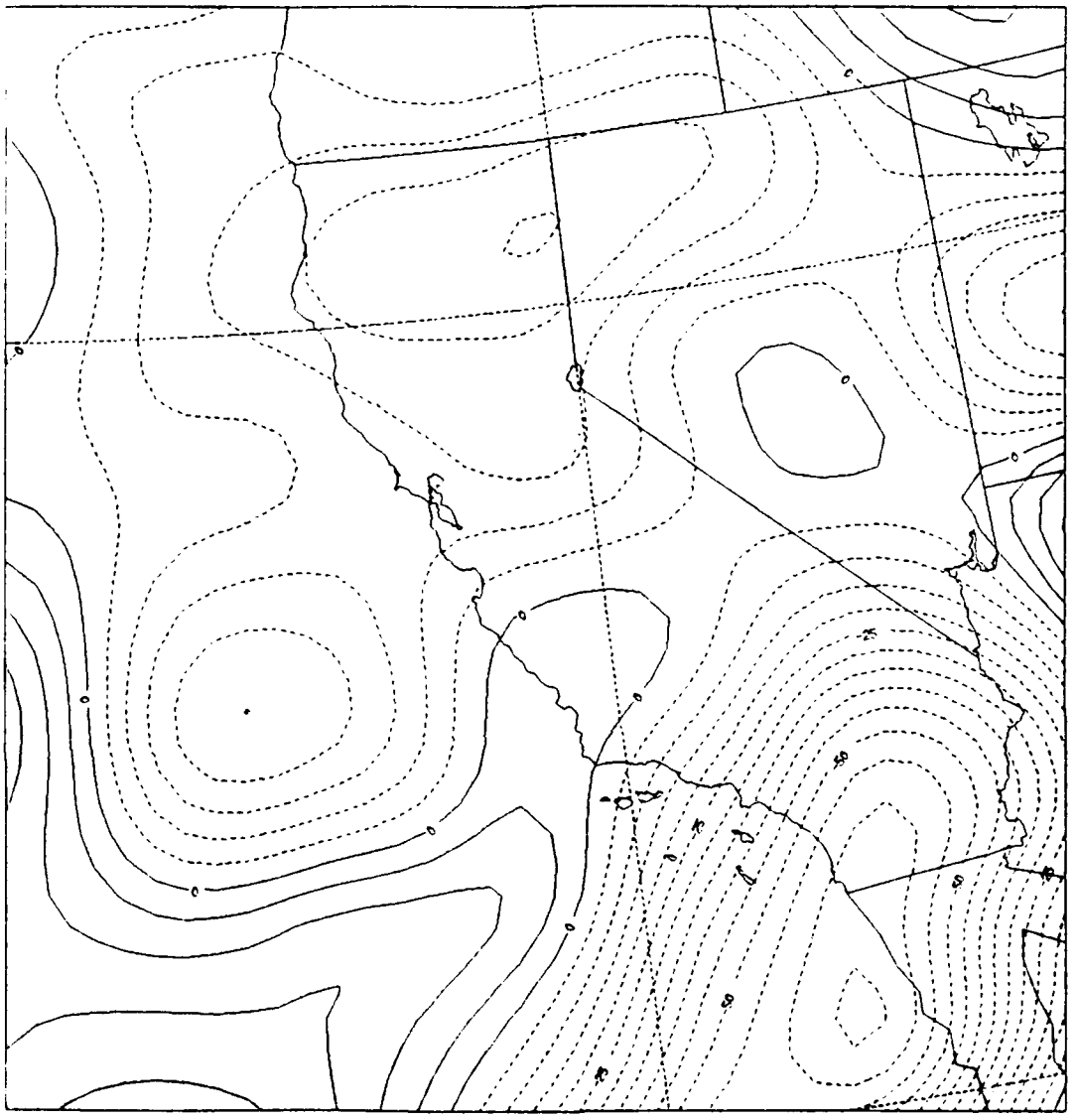

Figure 3. Synoptically forced 700 mb moisture flux ($u0f$). 1200 UTC 01 March 1991. Negative values correspond with upward flux.

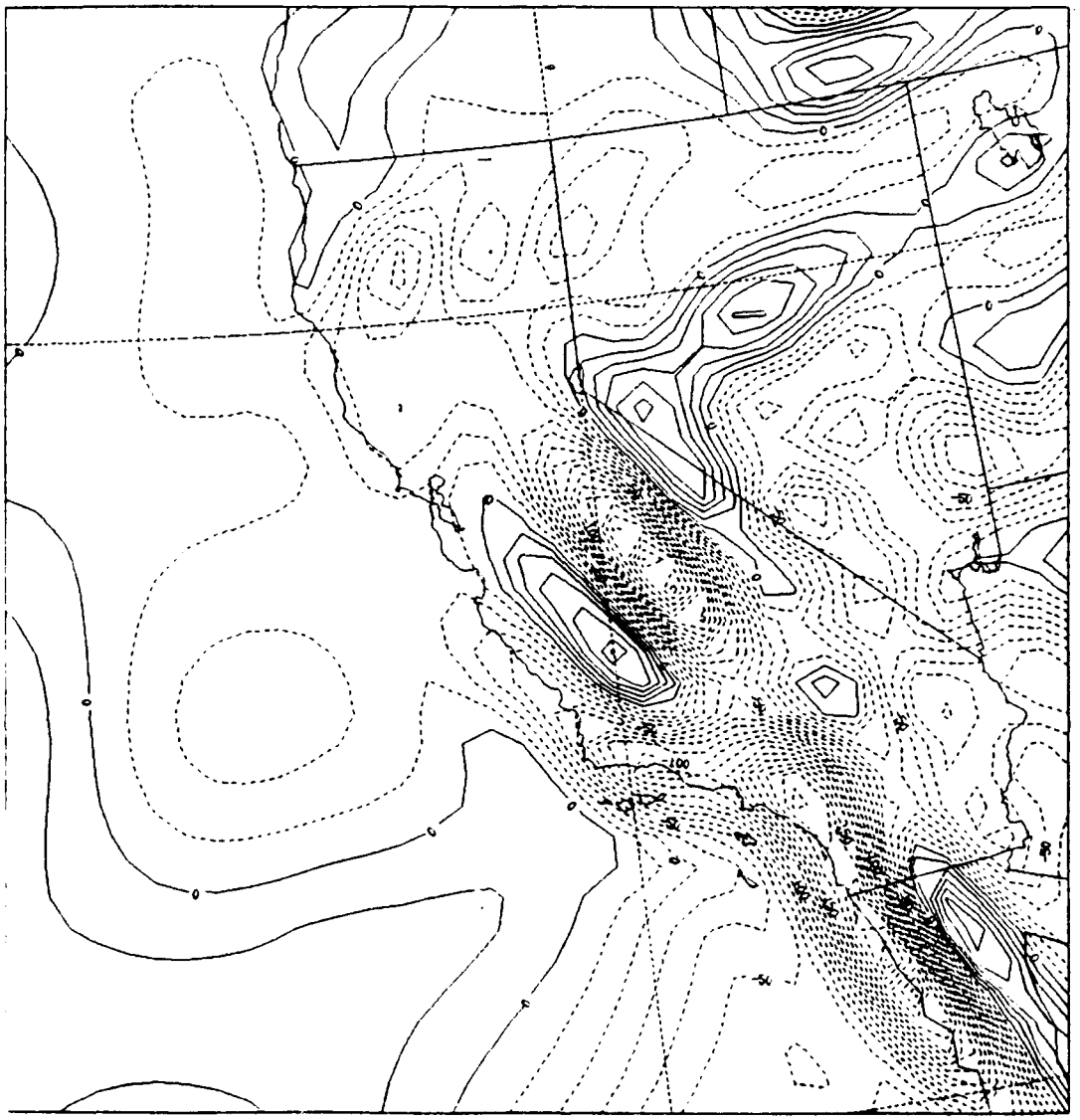

Figure 4. Total 700 mb moisture flux (*wqf*). 1200 UTC 01 March 1991. Negative values correspond with upward flux.

Specific rainfall totals obtained through hourly precipitation data publications (NOAA 1991) for the period of study were used to correlate precipitation with the *wqf* values. NOAA's precipitation totals consist of hourly rain gauge observations made at 244 locations within California. For our purposes, the observations have been grouped in six-hour increments exactly preceding and following the NMC analysis time. This gives 12 hour precipitation totals centered on the NMC analysis time which are then correlated with the corresponding *wqf* values.

IV. SYNOPTIC ANALYSIS

A. OVERVIEW

The series of synoptic-scale events that occurred during the period of this study were produced by the development of a 500 mb trough off the Northern California Coast. The system center migrated northeastward, over the period, and supported a series of short-wave troughs and associated surface cyclones (Figures 5 and 6).

An important factor in the synoptic evolution of this period is the movement of the primary jet stream. Approximately midway into the period (1200 UTC 02 March 1991), the jet repositioned itself over Central California, from the upper Baja Peninsula where it was located early in the period. This shift is evident in the 300 mb isotach analyses representative of the jet position at 1200 UTC 28 February 1991 and 0000 UTC 03 March 1991 (Figure 7). The jet axis shifts from a westerly to a more southwesterly orientation coincident with its latitudinal shift. As a result, the weather affecting California was dominated by highly baroclinic, fast moving cyclones in zonal flow with the surface center well poleward of the main jet early in the period, and weaker, less baroclinic systems late in the period, with only a brief transitional time in between.

As a consequence of the poleward migration of the jet, incoming weather systems affected more Northern sections of California late in the period, as evidenced by the 500 mb height rises observed over Southern California [illegible] mostly most of the

rain is concentrated in Southern California early in the period, with virtually no rain observed in Southern California by the end of the period.

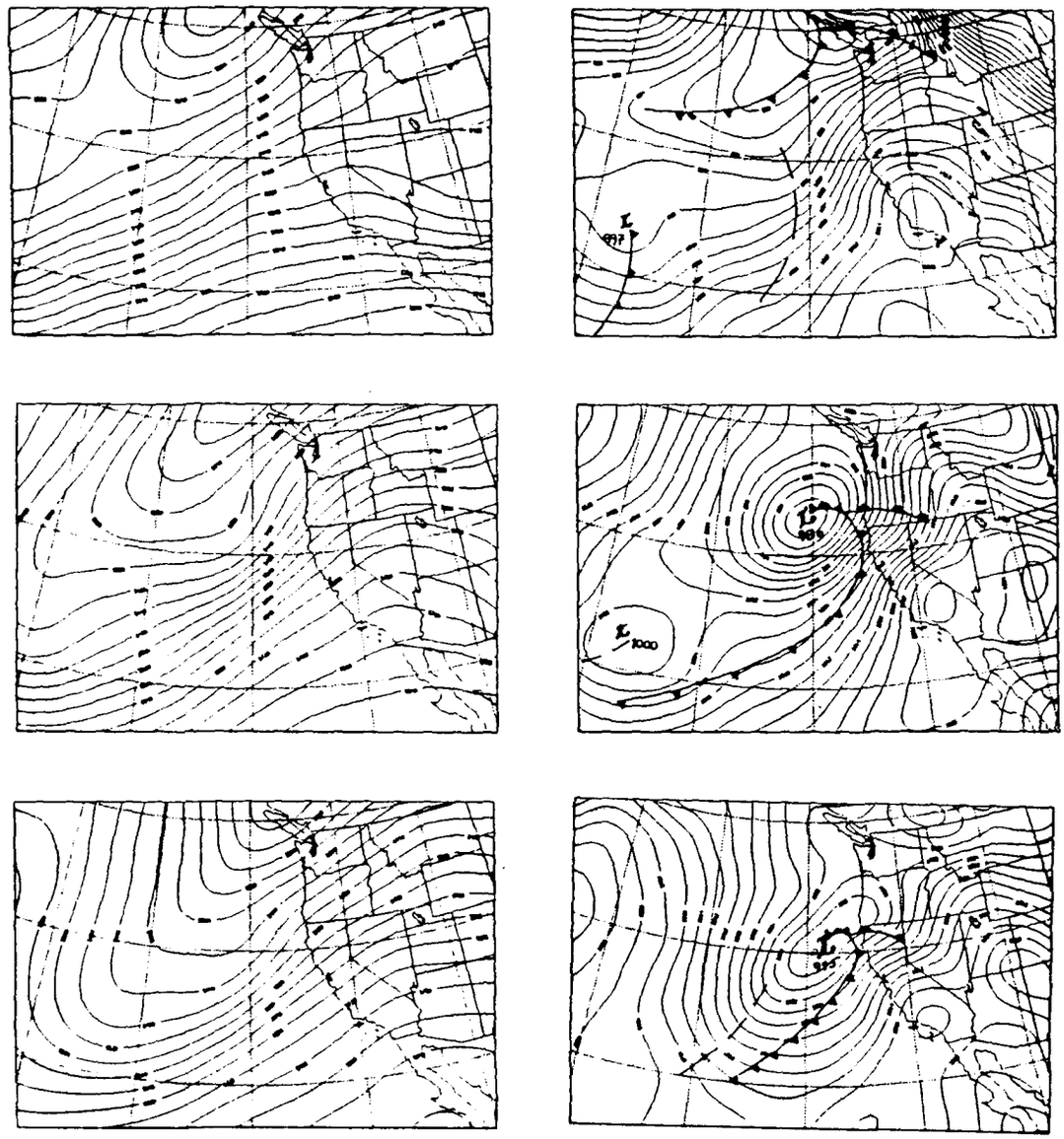

Figure 5. 500 mb heights (meters, left column) and surface pressure, including frontal positions (mb, right column) for (from top) 1200 UTC 27 February 1991, 1200 UTC 28 February 1991 and 1200 UTC 01 March 1991.

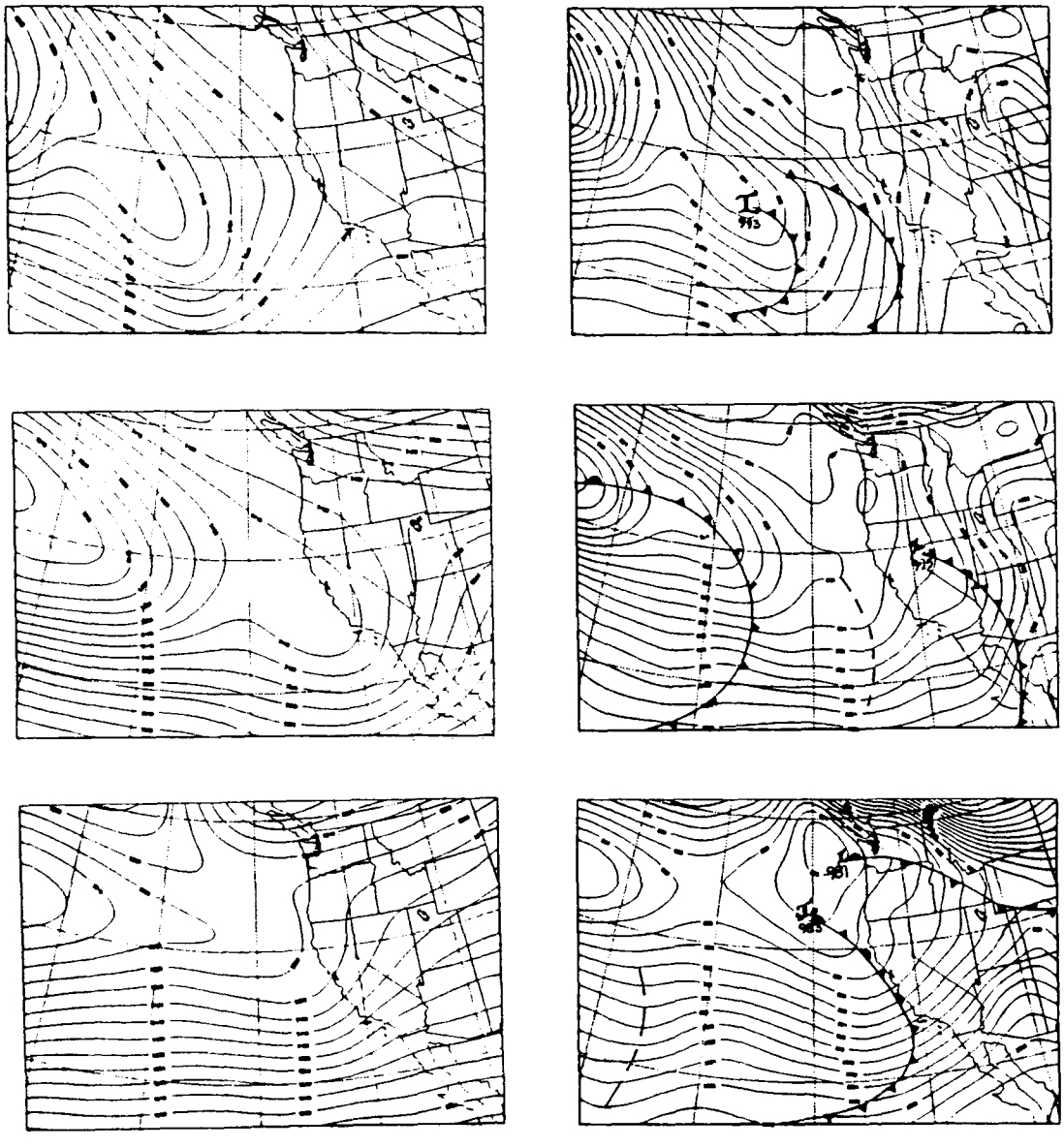

Figure 6. 500 mb heights (meters, left column) and surface pressure, including frontal positions (mb, right column) for (from top) 1200 UTC 02 March 1991, 1200 UTC 03 March 1991 and 1200 UTC 04 March 1991.

B. CYCLONE CHARACTERISTICS

1. 0000 UTC 28 February 1991 - 1200 UTC 02 March 1991

As mentioned, cyclones affecting the weather in California during this period developed on the cold, cyclonic side of the main jet, as seen in the GOES infrared imagery at 1200 UTC 28 February 1991 (Figure 8) over the Eastern Pacific and the corresponding mean sea level pressure and 1000-500 mb thickness analyses (Figure 9). This particular image and analysis are indicative of the general nature of the cyclones during this period. The strong surface thickness gradient along 30° N as well as the low-level instability upstream of the main frontal cloud bands on the GOES imagery indicate the strength of the baroclinic systems passing through California. These systems had significant pre-frontal cloud and precipitation bands associated with them. In general, this type of pattern is similar to that in which Collier (1975) applied his mesoscale enhancement model over North Wales, thus providing a good basis for comparison.

Cyclones of this nature are favorable for observing orographically enhanced precipitation, largely due to the forcing being well represented by the large-scale analyses and the precipitation primarily associated with the occluded front. However, post-frontal convection does pose a problem. While Collier (1975) applied his technique to rain associated with both cold and warm frontal passages, Bader and Roach (1977) tried to focus only on the mostly stable precipitation produced in the warm sector of cyclones. Browning *et al.* (1974) earlier concluded that orographically induced precipitation was most evident in the warm sector, as low-level [illegible] role during and

after cold frontal passage. Still, their results indicated orographic effects could be quantified even during and after the passage of the cold front. Results obtained by Collier (1975) showed less degradation of quantifiable orographic enhancement during cold frontal passage, as compared to warm sector precipitation, than did the results presented by Browning *et al.* (1974). Collier (1975) placed more emphasis on distinguishing between fast moving baroclinic systems in which mesoscale forcing is minimized, and slower, less baroclinic features as far as the observability of orographic precipitation enhancement. Since the cyclones in this period of the present study can be characterized as occluded surface features with mostly stable precipitation prior to frontal passage, and some post-frontal convection, orographic effects should be well represented. This study does not examine in detail the effect of mesoscale post-frontal convection on the overall correlation between wqf and observed precipitation.

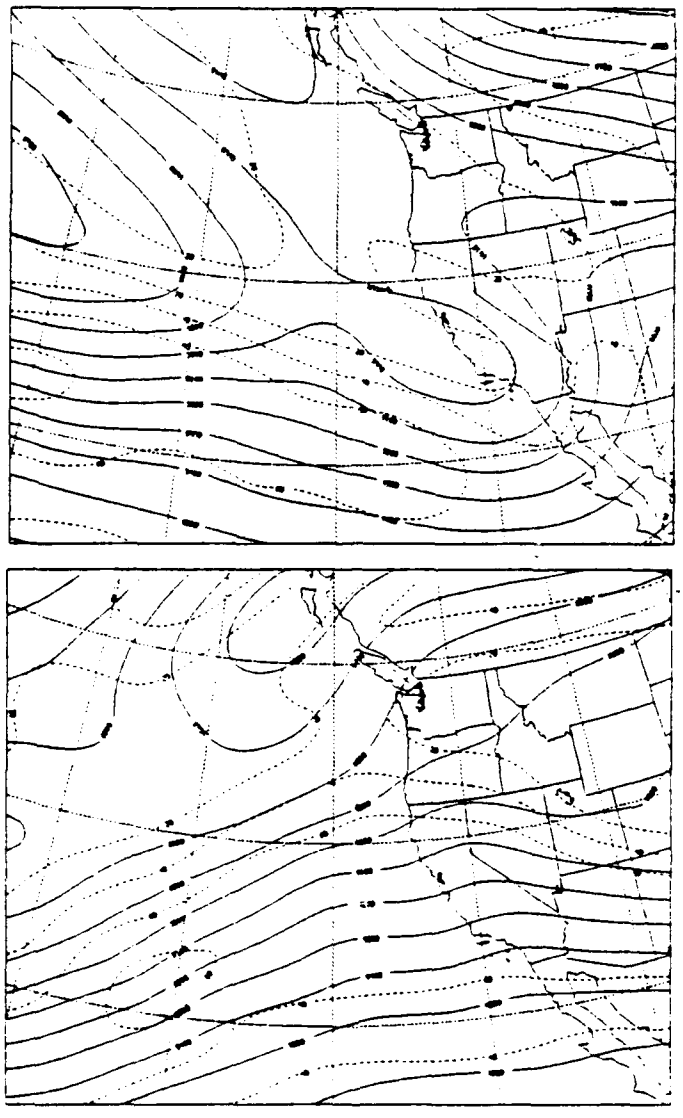

Figure 7. 300 mb heights (solid, meters) and isotachs (dashed, knots) for 1200 UTC 28 February 1991 (top) and 1200 UTC 02 March 1991 (bottom).

2. 1200 UTC 02 March 1991 - 1200 UTC 04 March 1991

The general nature of the three weather systems affecting California during this period is represented in Figures 10 and 11. The thickness gradient has shifted northward off the California coast and the amplitude of the pre-frontal thickness ridge is less than in the earlier cyclones. In addition there is a lack of post-frontal instability depicted on the infrared image. An exception to this pattern is the area of cloudiness at approximately 35° N, 150° W. As with the systems preceding it, this particular system becomes cut-off from the cold air within which it developed, and evolves mostly in response to the strong southwesterly flow aloft. This system (which reaches California at approximately 1200 UTC 04 March 1991), like the two seen ahead of it, has little representation of a thickness ridge ahead of the front as it reaches land. Without the pre-frontal baroclinic forcing, the rainfall associated with this type of system is less dominated by stable pre-frontal precipitation than cyclones in the earlier period. Due to the uninterrupted supply of warm, moist low- and mid-level flow from the southwest during this period, incoming weather systems produced less organized and more convective-type precipitation. This type of pattern was specifically avoided in terms of quantifying orographically induced precipitation by Collier (1975), since the forcing responsible for the distribution of precipitation was difficult to represent, even on the mesoscale. Consequently, this period of the present study may not be adequately represented by the synoptic-scale and orographic effects on precipitation.

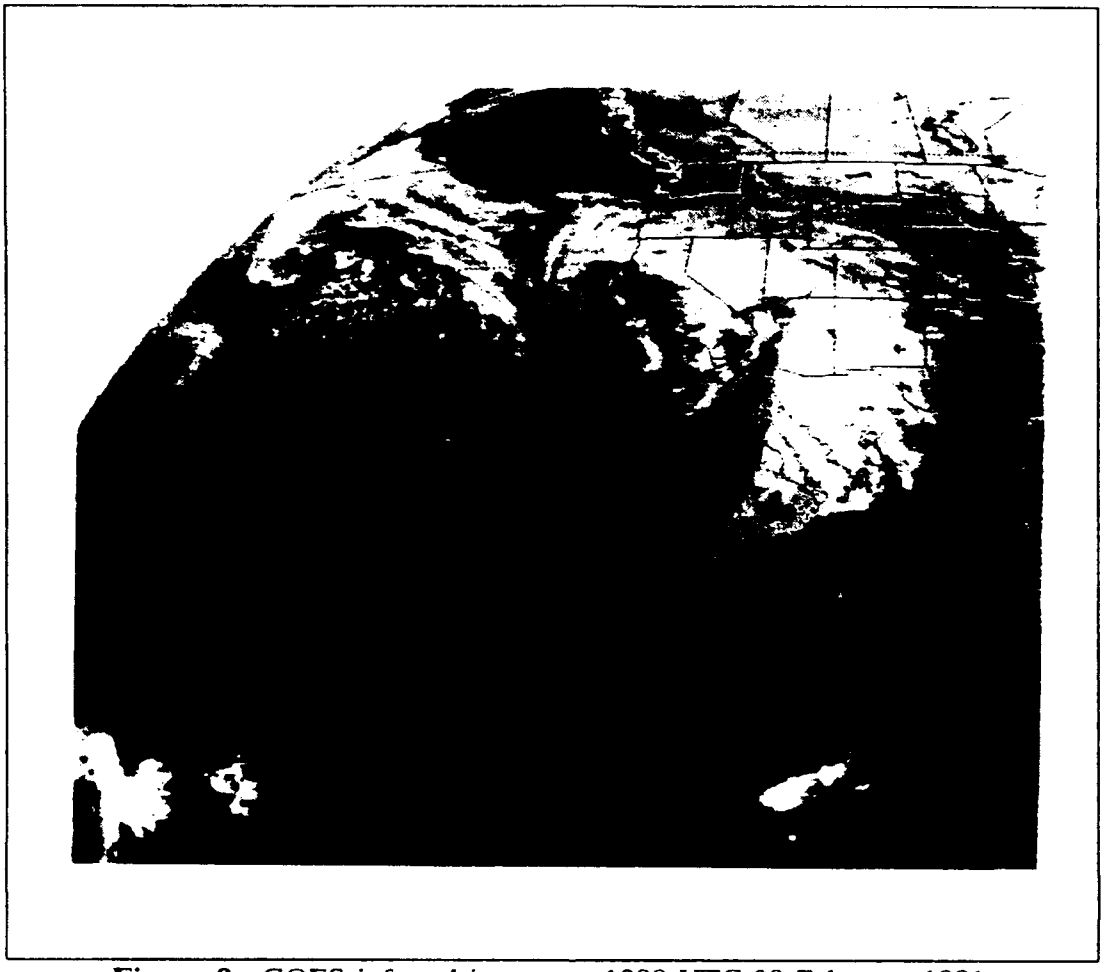

Figure 8. GOES infrared imagery. 1200 UTC 28 February 1991.

3. Summary

The above synoptic discussion suggests two cases that produced the observed rainfall distributions:

- Case (i) - strongly baroclinic cyclones with a well defined pre-frontal thickness ridge.
- Case (ii) - subtropically influenced convective complexes with little or no pre-frontal thickness ridge.

The first case tends to dominate the winter rainy season over California, although, the second case is not uncommon. Consequently, results from the two periods in this study cover contrasting synoptic conditions which produce rain in California.

V. RESULTS

A. OVERALL

1. Statistics

Table 1 shows the correlation, slope, and y-intercept from a linear regression analysis of *wqf* and observed 12 hour precipitation for four representative analysis times. The correlation values run from a virtually non-correlative -0.19 to a marginally respectable -0.55, as shown by the representative scatter plots in Figures 12 and 13. The correlation values are grouped at -0.2 and -0.5 for the later and earlier synoptic periods, respectively. This suggests that the synoptic and mesoscale factors discussed in the previous chapter predetermine the success of this technique to be either moderately correlative (-0.5) or essentially non-correlative (-0.2), with little in between. Averaging the slope and y-intercept of all "correlative" times (Table 1 shows just representative times) yields -0.010 and +35 respectively. Therefore,

$$\left[-(wqf)\times 0.01\right]+35=P \tag{6}$$

equates calculated *wqf* values with expected 12 hour accumulated precipitation (P), in inches. Note that all values of P *less than* zero represent a precipitation value of zero.

As will be shown in a later section, correlation is greatly improved in mountainous subregions as compared to the state-wide case. Since this technique is intended to be "universal" in its application to given subsynoptic scale parameters

and topography, (6) will be applied in all sub-regions, rather than deriving specific statistics for individual sub-regions.

TABLE 1. LINEAR REGRESSION STATISTICS (*WQF* VS. 12 HOUR PRECIPITATION)

	CORRELATION COEFFICIENT	SLOPE	Y-INTERCEPT (INCHES)
0000 UTC 28 FEB 1991	-.55	-.013	+0.50
1200 UTC 01 MARCH 1991	-.54	-.010	+0.35
0000 UTC 03 MARCH 1991	-.25	-.003	+0.40
1200 UTC 04 MARCH 1991	-.19	-.003	+1.00

One interesting statistical result is the fairly consistent y-intercept value for the linear regression of about +35 (average of six "correlative" times). This indicates that the precipitation threshold (the *x*-intercept) generally corresponds with slightly downward saturated moisture flux values. Though the smoothing process tends to distribute upward flux values into lee slope regions, it is still likely out-weighed by the "spillover" effect observed by Colton (1975). In this, spillover process, upward vertical velocities are advected over the summit region, effectively "mixing" upward vertical velocity air into lee regions. This process is not accounted for in the *wqf* calculation, which sees all lee regions as having downward velocities in the absence of synoptic scale upward motion.

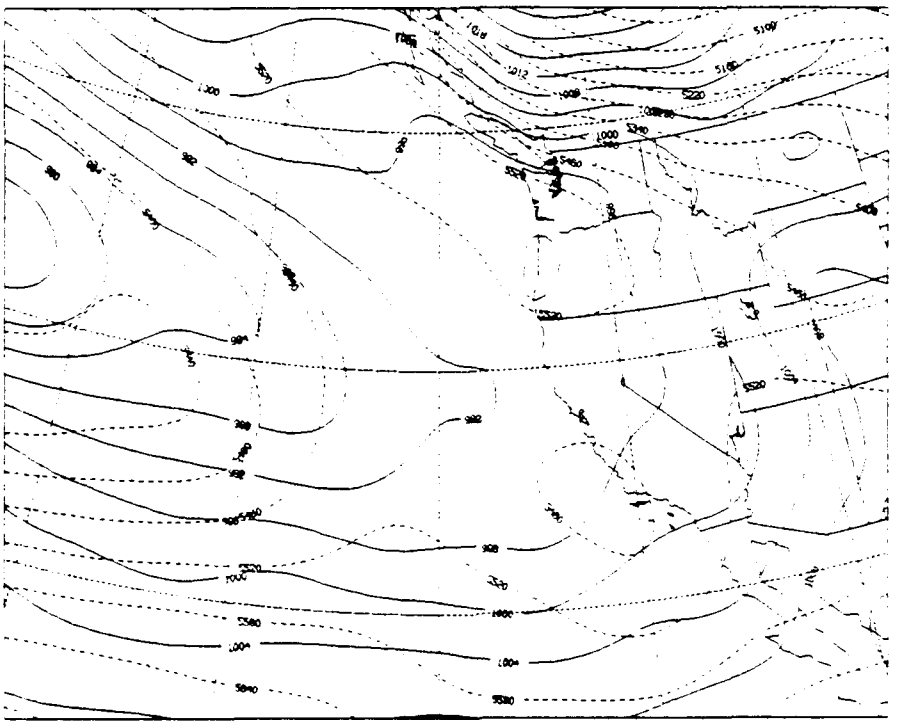

Figure 9. Surface pressure (mb, solid) and 1000-500 mb thickness (meters, dashed). 1200 UTC 28 February 1991.

Additionally, horizontal wind drift, as described by Collier (1975), may be producing artificially high precipitation

observations across summit regions, especially under conditions of strong low-level flow with a substantial perpendicular-to-barrier component.

The other consistent statistical feature is the slope value of either about -0.01 for the correlated times, or about -0.003 for times showing less correlation. This suggests a "flatter" precipitation distribution during non-correlative times, with non-orographic processes more dominant in forcing precipitation.

2. *Wqf* Distribution

Although the linear regression statistics computed above have a relatively low correlation, comparison of horizontal distributions of the *wqf*-inferred precipitation and observed precipitation reveals qualitatively correct distribution. In fact, this comparison reveals a significant improvement over NGM model forecast precipitation.

a. 0000 UTC 28 February 1991 - 1200 UTC 02 March 1991

Figures 14 and 15 depict the statewide precipitation distributions produced by *w0f* (the synoptic-scale forcing described in Chapter III), NMC's Nested Grid Model (NGM) forecast precipitation for 1200 UTC 28 February 1991, actual observations and *wqf*. Of note here is the similarity between the NGM forecast precipitation and the *w0f* field, particularly the maximum over Southern California. This implies that the synoptic forcing we are using in our calculations of *wqf* bears rough equivalency to the NGM precipitation. This time is especially informative since the 12 hour 700 mb vertical velocity forecast verifies particularly well compared to the kinematically calculated analyzed 700 mb vertical velocity (not shown). It should be mentioned that *w0f* showed virtually no correlation with observed precipitation throughout the study.

In general, we see a significantly greater amount of detail within the precipitation field produced by *wqf*, compared to either *w0f* or the NGM forecast. Also note the "false" maxima produced in the observed field. This is mainly a result of the multiquadrant contouring technique extrapolating basis functions into regions of sparse data (i.e., Mojave Desert, and over the ocean). The [illegible] of the *wqf*

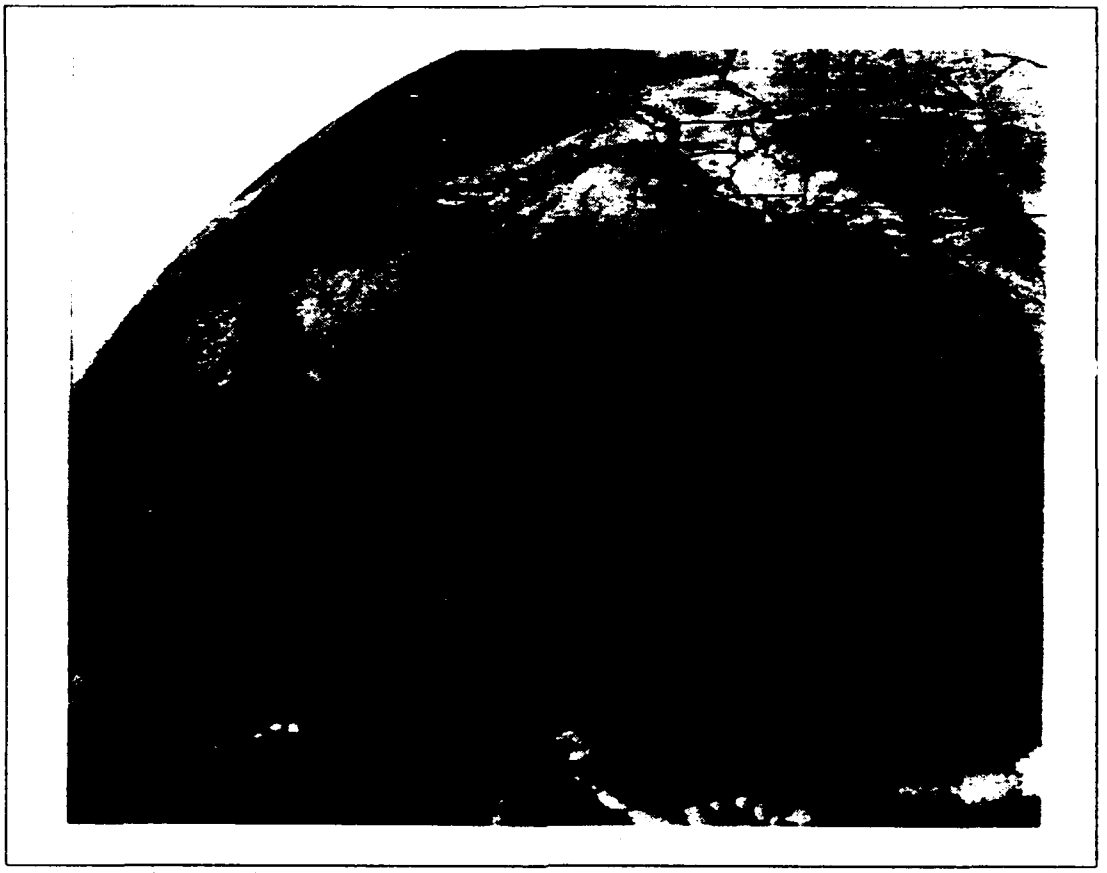

Figure 10. GOES infrared imagery 1200 UTC 02 March 1991.

distribution reflects the observations reasonably well, particularly the maxima observed over the mountains of Southern California and the Sierra Nevada. Note that correlations are performed between the gridded *wqf* fields and station locations (rather than gridded precipitation). It should be noted that overall correlation is generally constant from 0000 UTC 28 February 1991 to 0000 UTC 01 March 1991, with the exception of time 0000 UTC 01 March 1991, which has a correlation coefficient of -0.21. This drop in correlation is most likely in response to the low-level convection seen in Figure 8 located between the main frontal bands. This pattern [illegible] studies, that

post-frontal precipitation distribution is determined less by orography than convective processes.

b. 1200 UTC 02 March 1991 - 1200 04 March 1991

Figures 16 and 17 depict the same parameters as Figures 14 and 15 except for 1200 UTC 04 March 1991, which is representative of the second period. Here *wqf* is generally a less accurate representation of observed precipitation, particularly along the Central California Coast. Still, orographic maxima produced by *wqf* over the mountains of Northern California and the Northern Sierra Nevada are reasonably representative of observed maxima. Though the corresponding NGM precipitation forecast shows good areal coverage, it is devoid of any of the above structure. In this case the NGM vertical velocity forecast, on which precipitation is largely based, shows a strong area of upward motion located over Northern California, whereas the verifying kinematically calculated analysis shows this area of upward motion to remain off-shore (not shown). As such, the NGM precipitation field owes its accuracy more to chance than to improved dynamical representation. It seems that neither the NGM forecast or the GDAS analysis fields are able to pick up on the forcing responsible for the locally heavy rainfall in this period. Referring back to Figure 6, we see an analyzed "front" off the Northern California coast at this time, with most of the state within the warm sector. A random check of station observations supports the strong southerly flow depicted by the GDAS analyses. Convective lifting would, in this case, be the best explanation for the lack of upward vertical velocity in the [illegible] noted

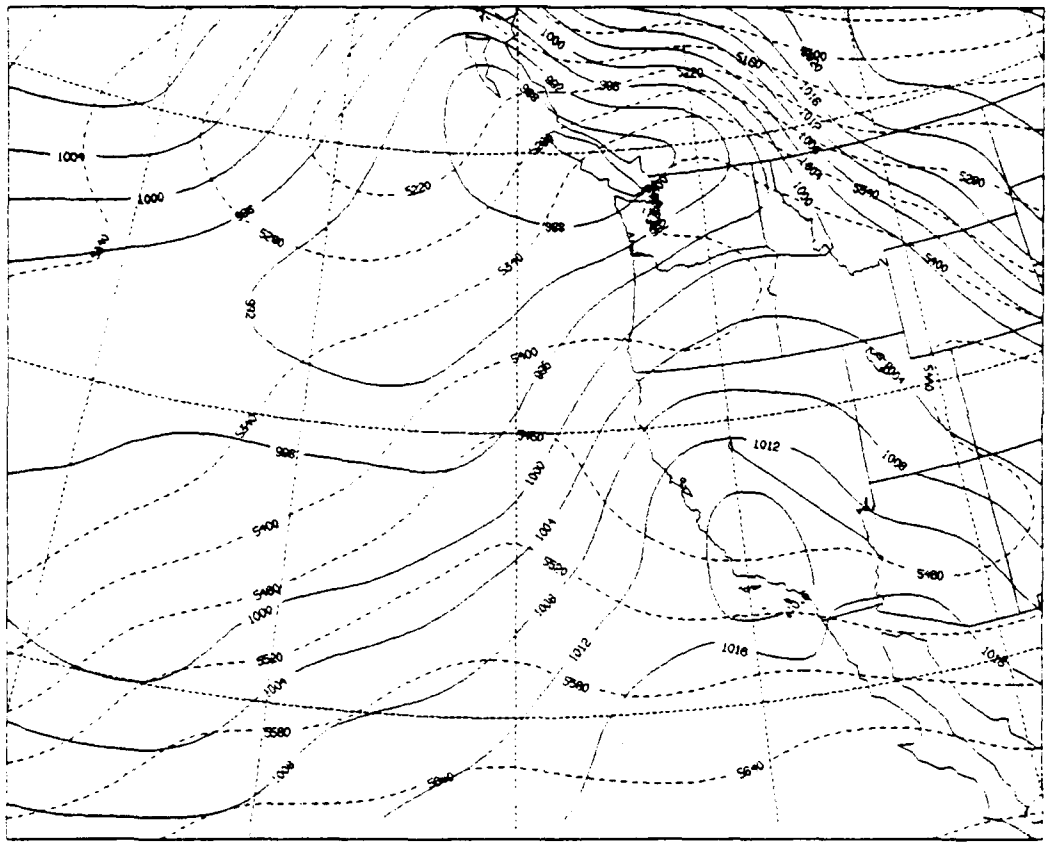

Figure 11. Surface pressure (mb, solid) and 1000-500 mb thickness (meters, dashed). 1200 UTC 02 March 1991.

earlier, this period is dominated by only marginally baroclinic features in the moist southwesterly flow aloft. As such, convection is likely to be equally important in both the pre- and post-frontal periods. Though convective processes are parameterized in the NGM precipitation forecasts, they are not accounted for at all in the calculation of *wqf*.

3. Correlation Limiting Factors

a. Synoptic Conditions

As described by Collier (1975), synoptic conditions favorable for observing orographic enhancement of precipitation are characterized by fast moving baroclinic systems. The thinking is that slower moving, or non-baroclinic systems allow more non-orographic and/or mesoscale mechanisms to influence rainfall distribution. This is not to say that topography does not influence mesoscale structure. Rather, since only the large-scale structure is considered, topography is only allowed to influence the synoptic-scale fields. As mentioned previously, the period prior to 1200 UTC 02 March 1991 was characterized by baroclinic features well represented by the synoptic fields, whereas non-orographic and/or a mesoscale processes dominated after this time. The statistical correlations support this characterization of the dominant precipitation type during the periods. However, as seen in the horizontal distribution of *wqf* during the second period, the qualitative distribution of precipitation is realistic in the second period. This suggests that the amount of precipitation is poorly represented in more convective-type periods, but the general distribution is still strongly influenced by the topography.

b. Smoothing

Aside from subgrid-scale effects, smoothing of the topographic w used to calculate $(\omega q)_{P_0}$ seems to be most detrimental to correlation values. As previously discussed, "mesoscale" orographic forcing produced by synoptic-scale 1000 mb winds over 40 km resolution topography required [illegible] smoothing to be

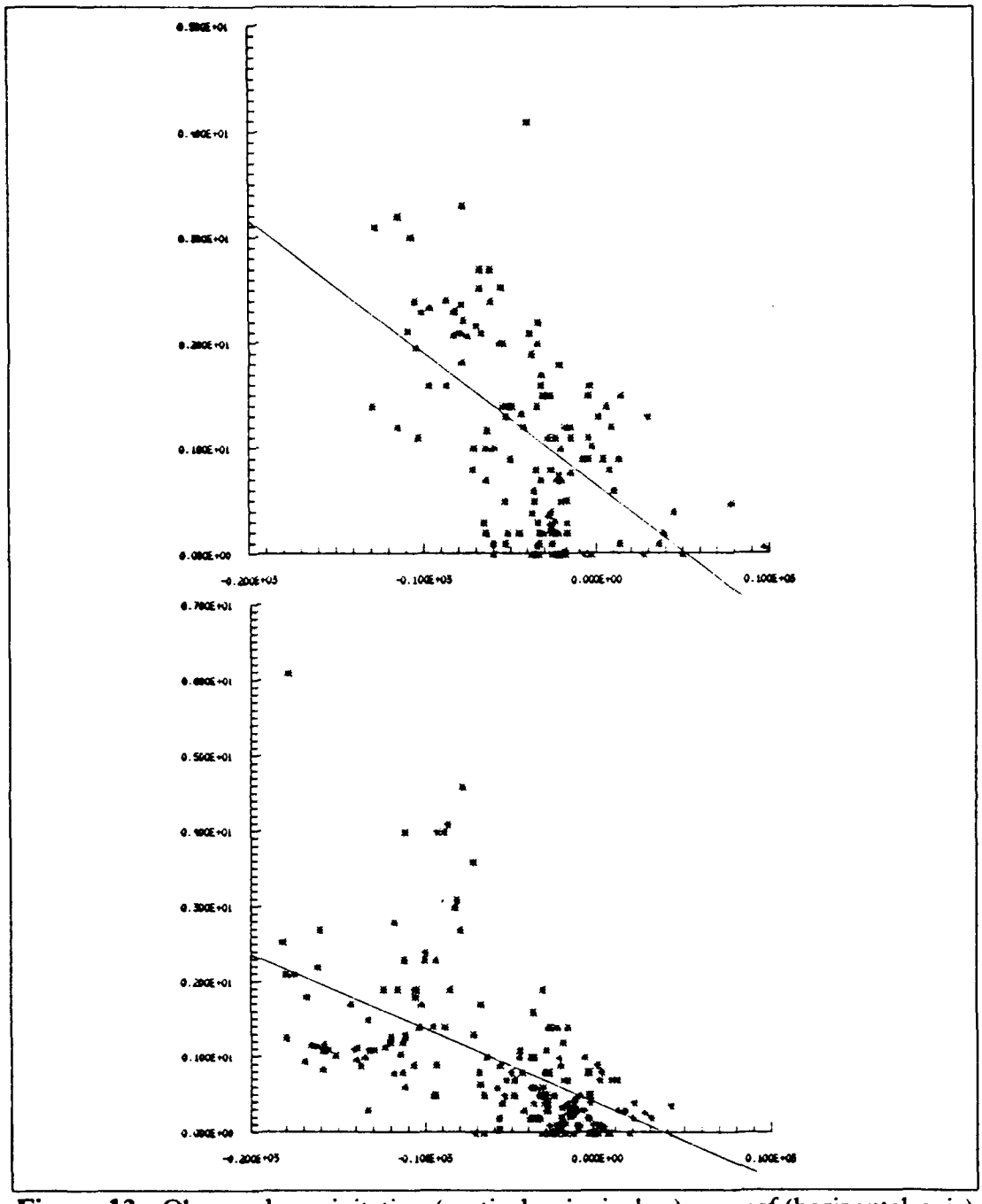

Figure 12. Observed precipitation (vertical axis, inches) vs. *wqf* (horizontal axis) and calculated linear regression for 0000 UTC 28 February 1991 (top) and 1200 UTC 01 March 1991 (bottom).

compatible with the synoptic-scale forcing. As a result, stations upwind of topographic barriers, such as Fresno (station FRES, Figure 18) are generally assigned *wqf* values far in excess of the actual calculated forcing. Note (Figure 18) that the smoothed *wqf* value for FRES (-15) is nearly twice that of the unsmoothed value (-8).

c. Location

Certain locations, such as coastal areas, are more likely to have higher actual relative humidities than inland areas, which are analyzed as equal on the synoptic-scale. As a result, more of the vertical moisture flux *wqf* is likely to be converted to precipitation in coastal areas than inland areas, where a larger amount of moisture flux (*wqf*) may be required to maintain or reach saturation. This relationship is evident in comparing the linear regression corresponding to the San Bernardino - San Gabriel subregion (subregions are defined in the following sections) to that of the Southern Sierra Nevada (Figure 19). Note that a *wqf* value of -100 represents approximately a 2.75" 12 hour precipitation accumulation according to the linear regression derived for the San Bernardino/San Gabriel subregion, but less than 1.0" based on the Southern Sierra Nevada subregion's statistics.

d. Other Considerations

Obviously, numerous other considerations affect the correlation of precipitation and 700 mb saturated moisture flux. Redistribution of moisture above 700 mb, quantification of evaporation, and wind channeling induced by the topography are a few examples. Though important, such processes cannot be easily accounted for on the synoptic scale. In fact, these factors will require more specific consideration if *wqf* cannot adequately represent the forcing patterns which lead to precipitation distributions in mountainous regions.

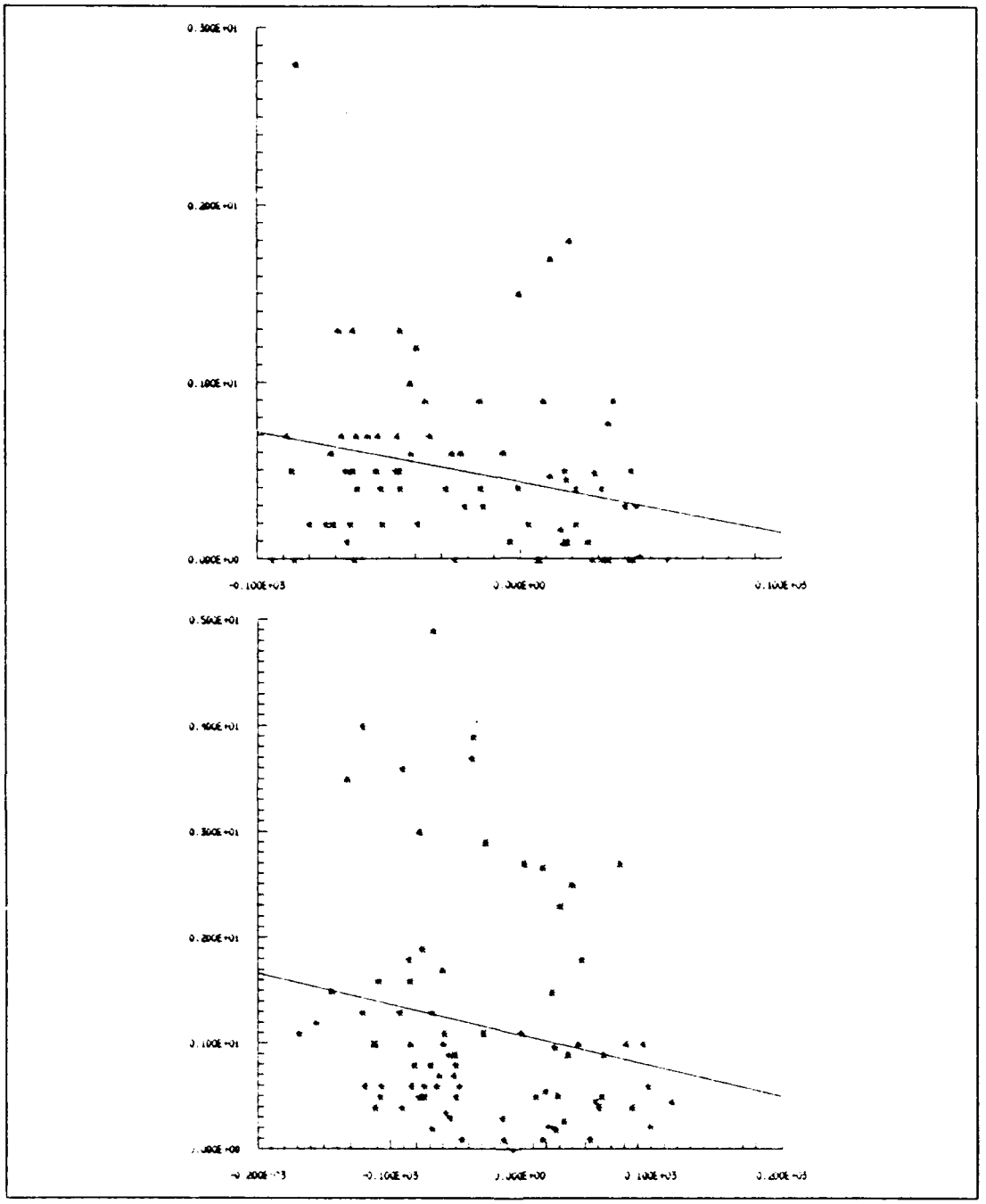

Figure 13. Observed precipitation (vertical axis, inches) vs. *wqf* (horizontal axis) and calculated linear regression for 0000 UTC 03 March 1991 (top) and 1200 UTC 04 March 1991 (bottom)

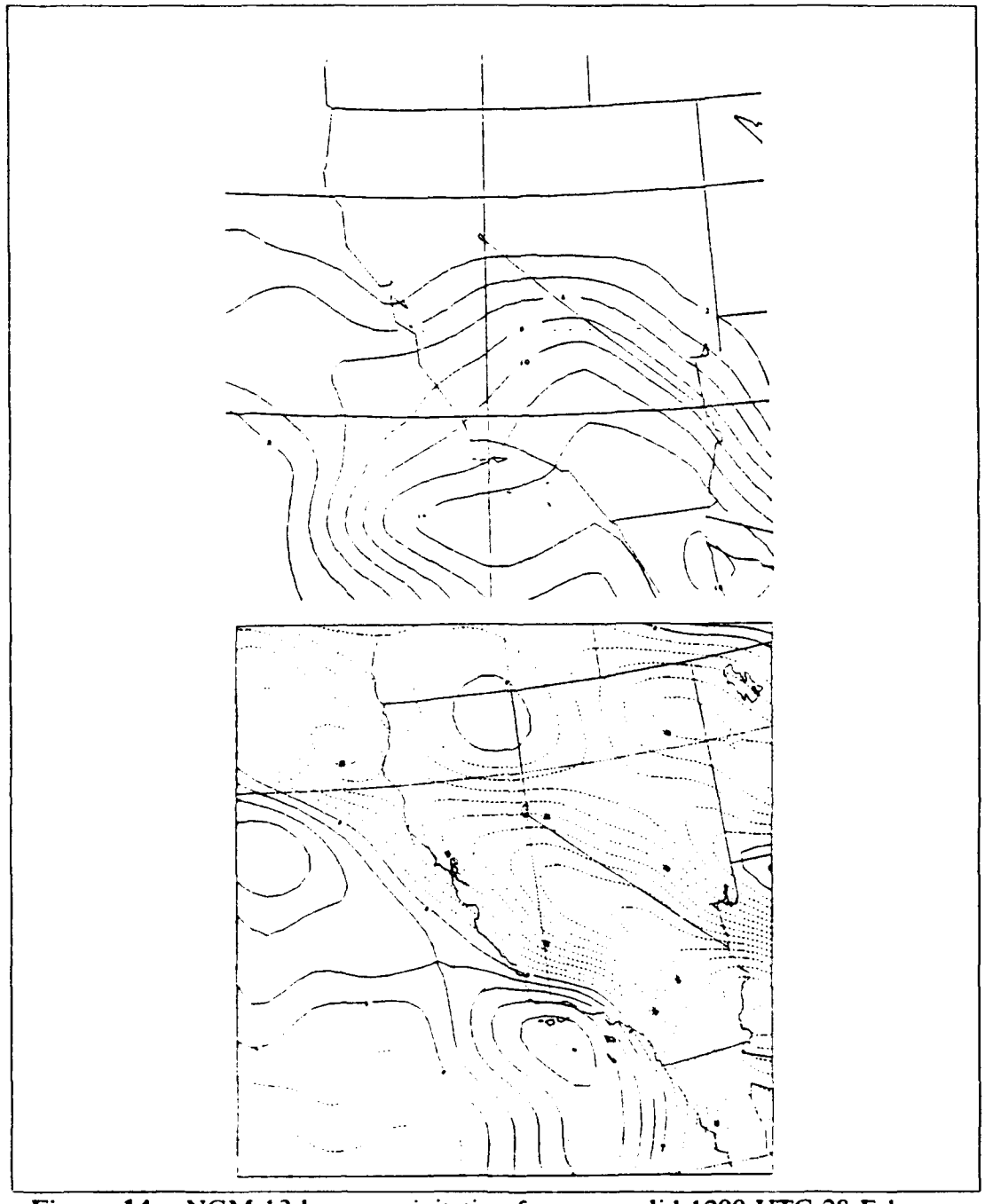

Figure 14. NGM 12 hour precipitation forecast, valid 1200 UTC 28 February 1991 (mm, top) and $w\sigma f$ (bottom) for 1200 UTC 28 February 1991.

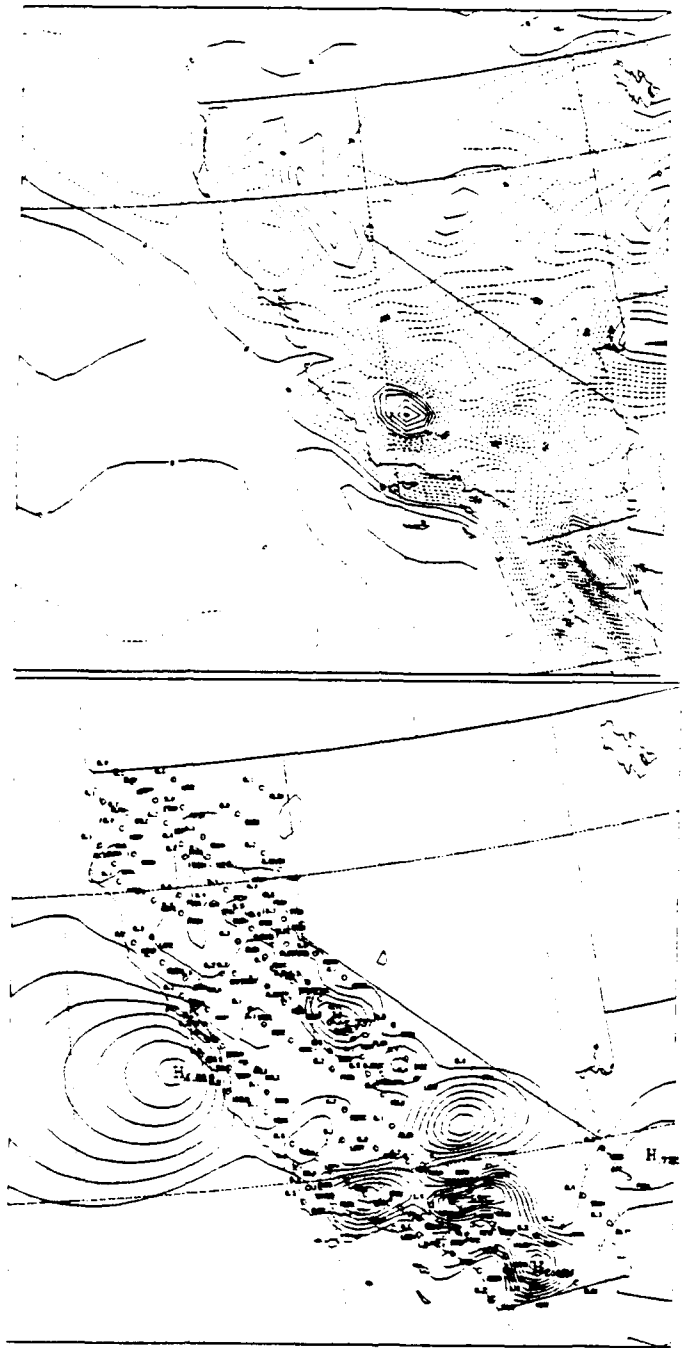

Figure 15. *Wqf* for 1200 UTC 28 February 1991 and observed precipitation (inches, bottom), 0600 UTC 28 February 1991 - 1800 28 February 1991.

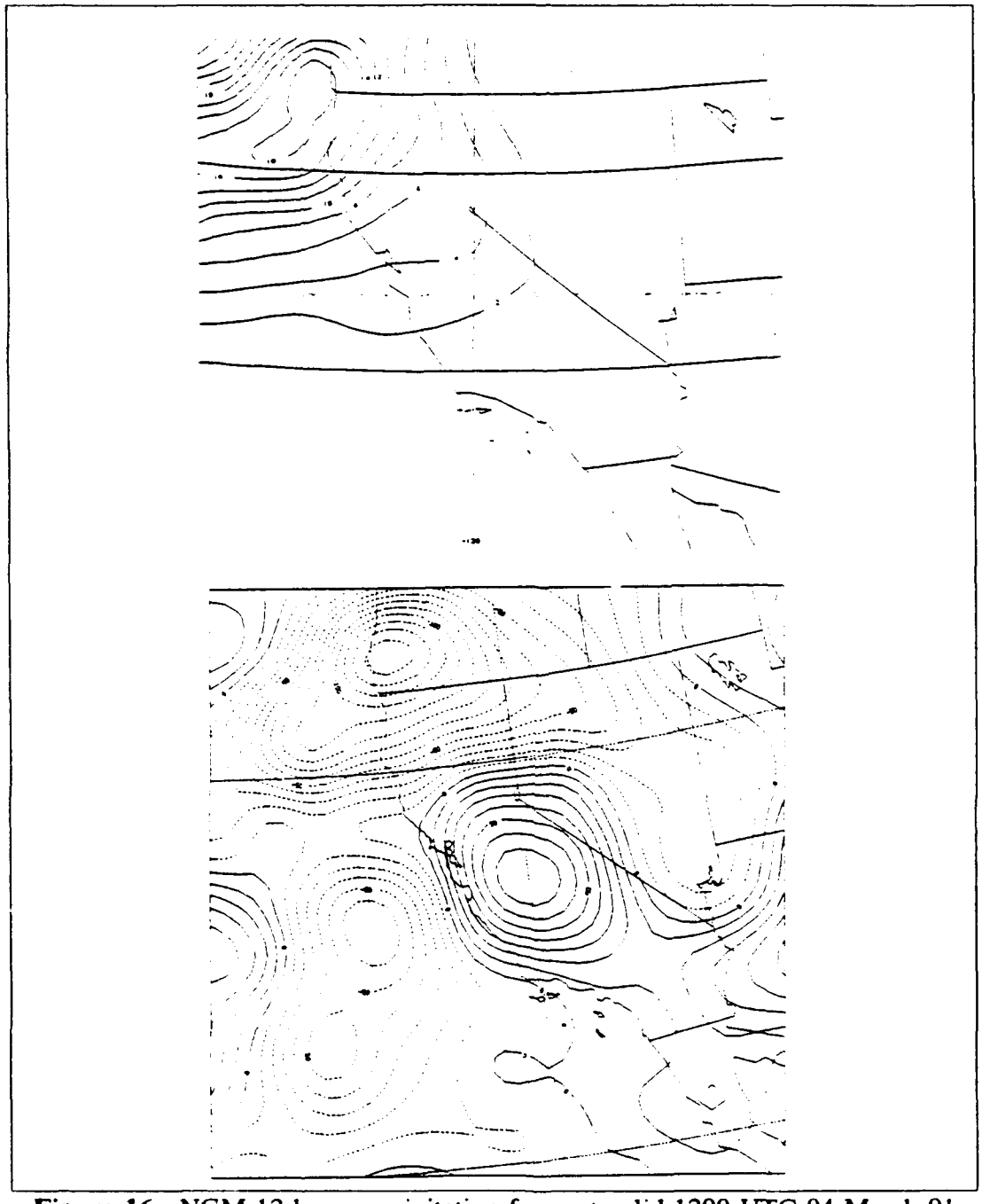

Figure 16. NGM 12 hour precipitation forecast valid 1200 UTC 04 March 91 (mm, top) and $w0f$ (bottom) for 1200 UTC 04 March 1991.

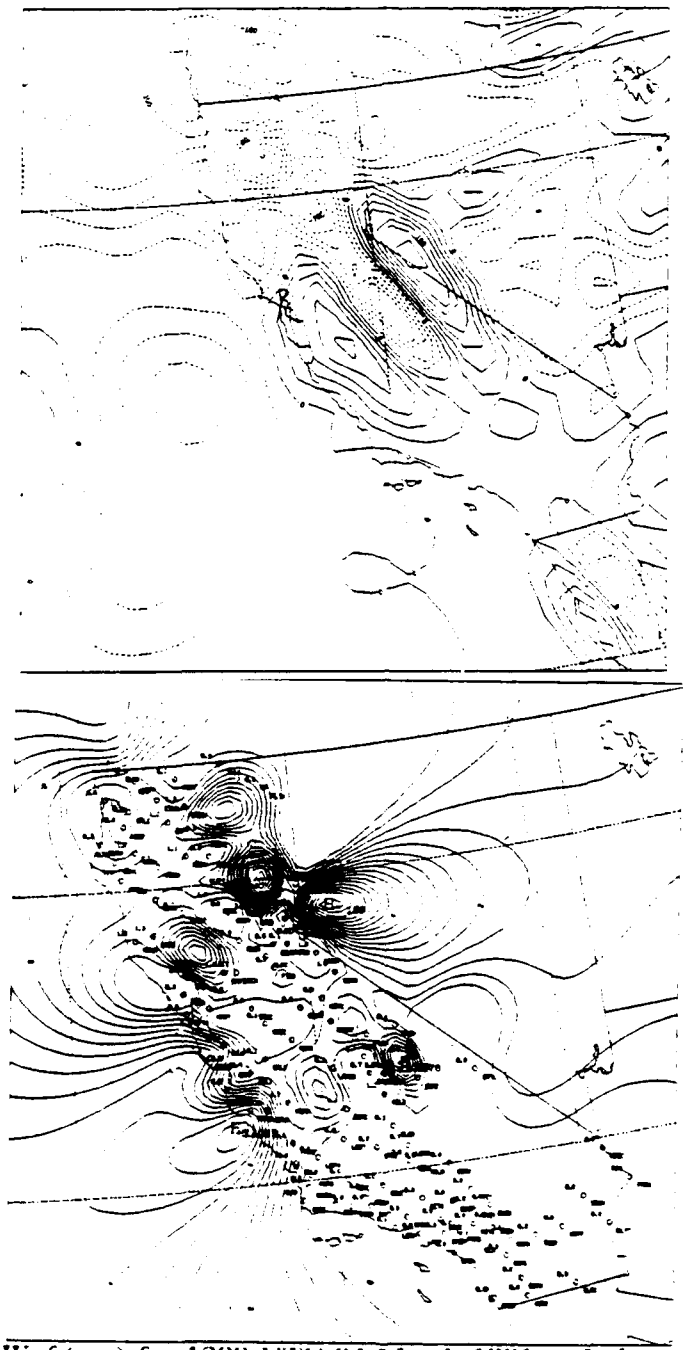

Figure 17. $\overline{Wqf}$ (top) for 1200 UTC 04 March 1991 and observed precipitation (inches, bottom), 0600 UTC 04 March 1991 - 1800 UTC 04 March 1991.

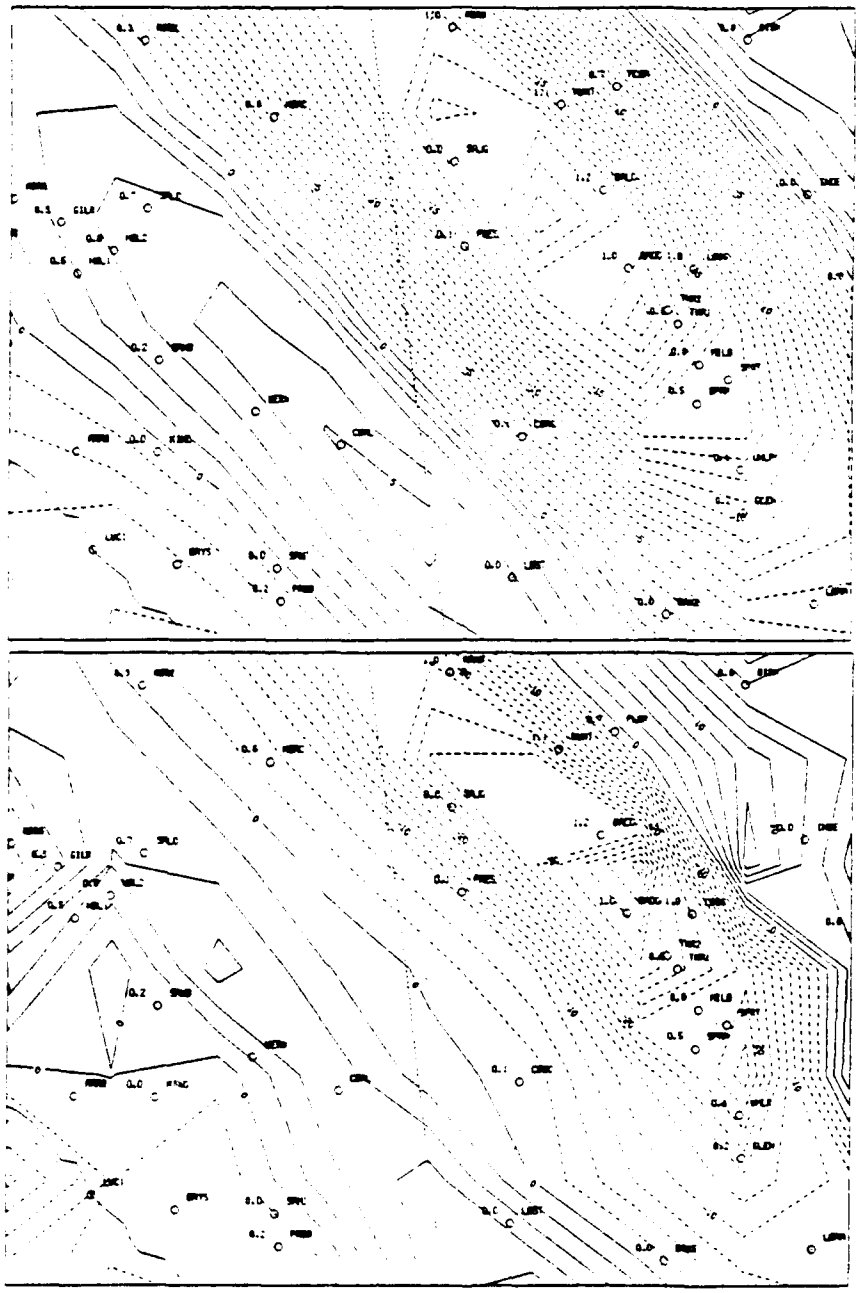

Figure 18. Unsmoothed (top) and smoothed (bottom) orographically forced vertical velocity (cm/s). 0000 UTC 01 March 1991.

B. REGIONAL

1. Approach

While the general results are indicative of the overall value of the *wqf* parameter in representing precipitation over a wide region, it is perhaps more important to determine the extent to which the correlation can be improved when applied to a specific topographic region. In this way, *wqf* may be able to identify specific regions or even drainage basins likely to receive heavy precipitation under certain forecast conditions. For this reason, the specific performance of *wqf* in regions of well defined topography is examined to determine the ability of *wqf* to represent precipitation in specific regions. In effect, the extent to which synoptically derived low-level winds interacting with topography can represent the mesoscale distribution of precipitation within mountainous regions will be determined. Little or no improvement of the regional correlation coefficient over the general case would suggest limited usefulness of the synoptic-scale winds in determining orographic forcing. An increase in correlation would, however, indicate that a significant component of the precipitation forcing is due to the large-scale wind field interacting with regional topography, and that this quantity is more easily isolated in regions of well defined topography. Specific correlation coefficients are presented as required in each subregion.

The regions chosen for this specific purpose all have topography which is relatively well represented at 40 km resolution. In each case, regions are defined by the particular topographic features being [illegible]. Results are

presented by showing the observed precipitation across a topographic cross-section which is chosen based on observational density as well as topographic gradient. Observations are then compared to the *wqf* derived quantities. Topography requiring finer resolution to be represented does not fare well, as smoothing tends to destroy the forcing maxima (a good example is the Santa Cruz mountains). As much as possible, limitations, as well as strengths, corresponding to specific regional correlation will be identified.

2. Topographic Subregions

a. San Bernardino/San Gabriel

This subregion was particularly hard hit by storms early in the period. Figure 20 shows the regional topography to consist of a broad flat area bordered to the northeast by the abrupt rise of the San Bernardino range. Figure 21 shows the actual observed precipitation accumulations along with the *wqf* derived quantities, for 0600 UTC -1800 UTC 01 March 1991 combined with a representative cross-section of the regional topography. This particular cross-section is representative of the general correlation within this subregion, and was chosen since it represents the period of maximum rainfall.

The *wqf* parameter seemed to do a particularly good job handling the Mojave Desert stations throughout the period, while showing only moderate success in the upslope regions. This may best be explained by the coarse resolution of the topography southwest of the crest. Our technique sees only a broad, continuously sloping

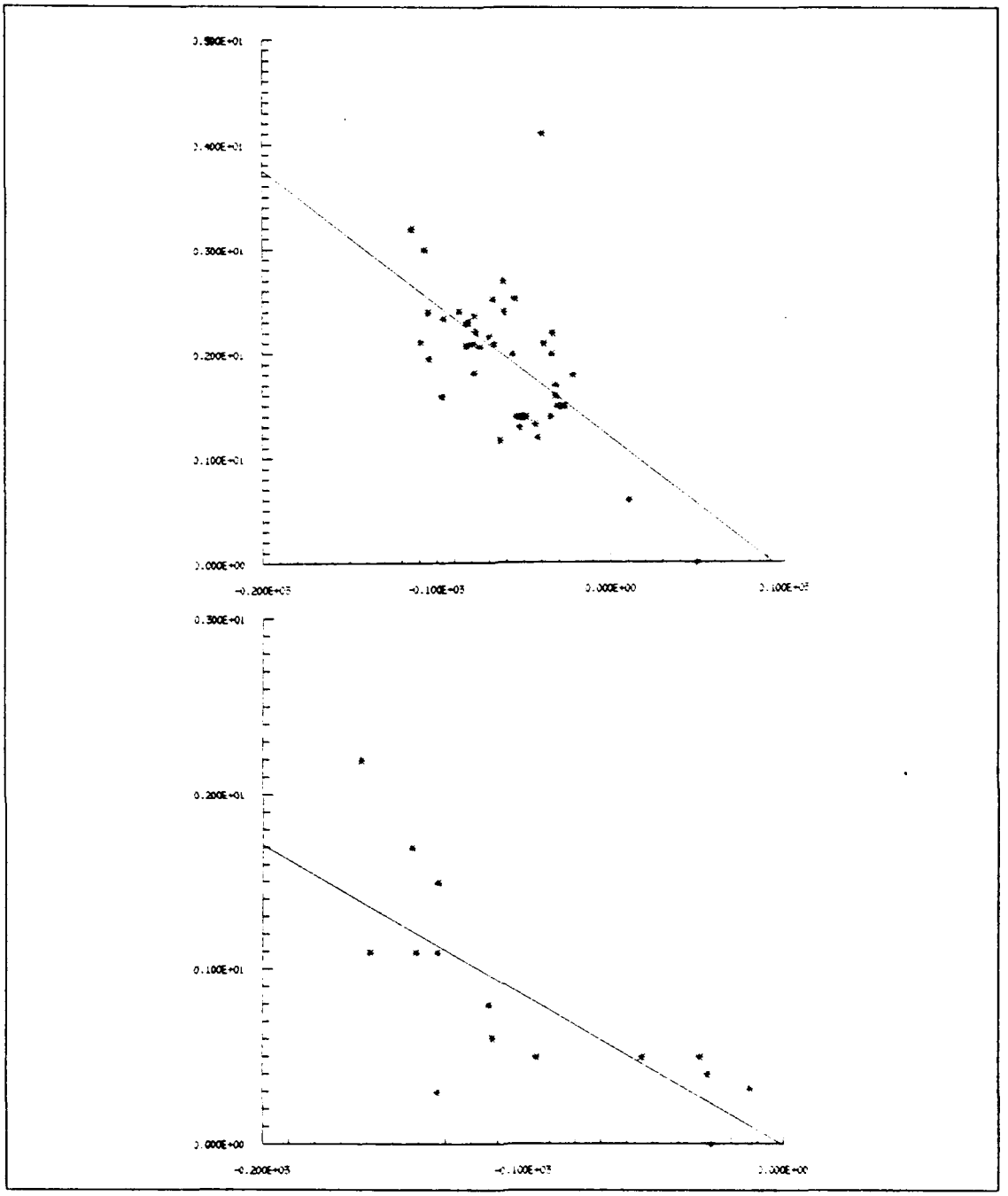

Figure 19. *Wqf* vs. observed precipitation (inches, vertical axis) for San Bernardino/San Gabriel subregion (0000 UTC 28 February 1991, top) and Southern Sierra Nevada subregion (1200 UTC 01 March 1991, bottom).

region, whereas many reporting stations lie in dissected valleys (i.e. Riverside at 301 m is assigned an elevation of 550 m by the 40 km topography). Also note (stations 1, 2 and 3 on Figure 21) the inflated *wqf* values close to the ocean. This results from the smoothing process described earlier.

With some notable exceptions (i.e., Lytle Creek Ranger Station (LYCR #11)), *wqf* does a decent job of representing the regional precipitation showing a 10% increase in the correlation coefficient over the state-wide case. Forcing responsible for the anomalous observations (i.e., LYCR and CRES) is certainly of too small a scale to be accurately accounted for by this technique. Still, the ability of *wqf* to correctly produce a specific area of heavy precipitation (>1.5" in 12 hours), as well as define the lesser amounts observed in the Mojave Desert (stations VICT, BORO, DAGG and MOJA) is encouraging. By comparison, NGM 12 hour precipitation totals forecast for this region were all less than 0.4 inches with no upslope or lee structure in the NGM precipitation (not shown).

Of course, *wqf* has the benefit of being statistically fitted to actual observations, where the NGM forecast represents a strictly physical quantity. Nonetheless, the statistical fit achieved by *wqf* is derived objectively, and is intended to be applied in all conditions. Still, an application of this method to *independent* data is needed to determine predictive skill.

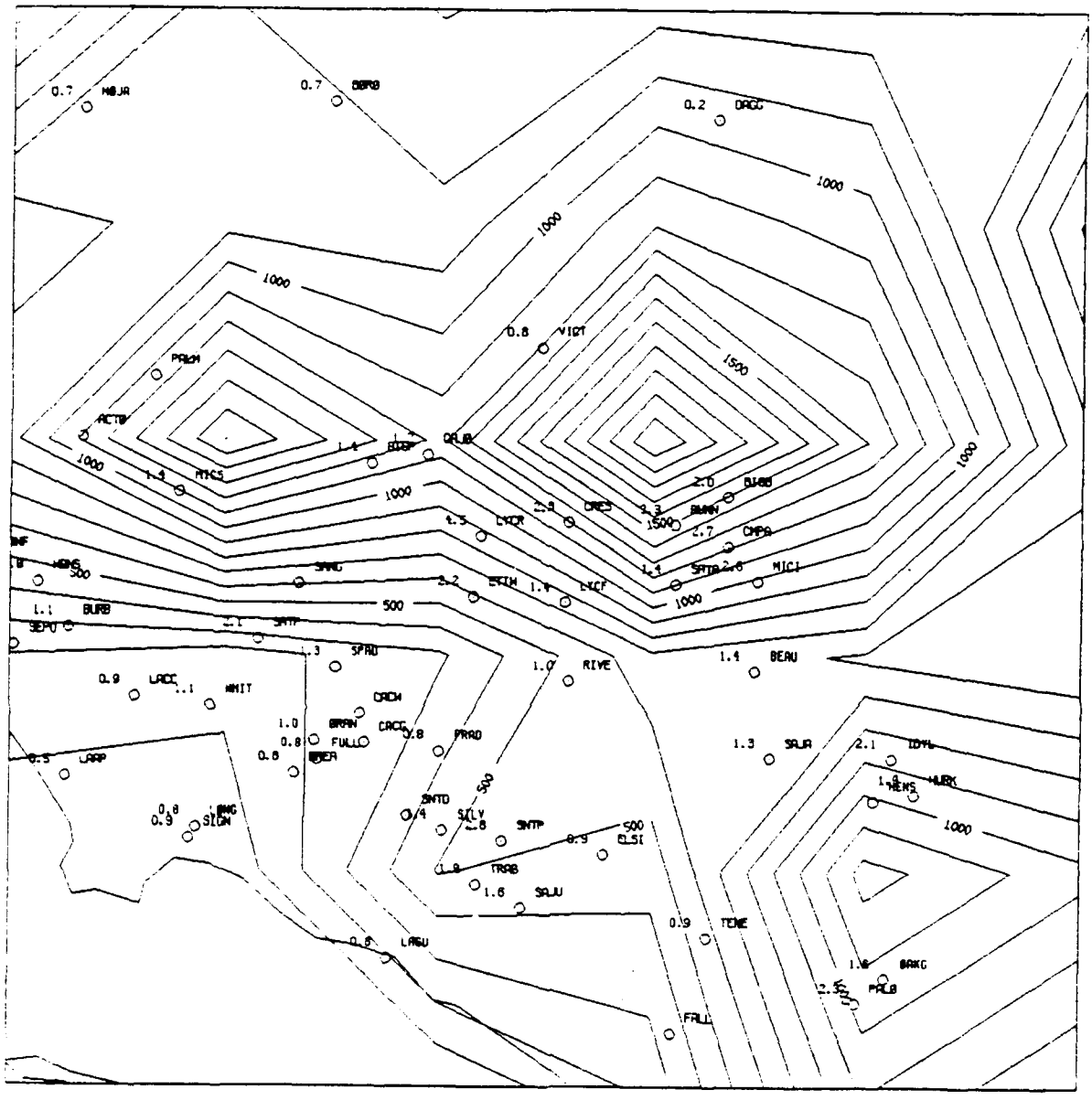

Figure 20. Topography (meters) and station names for San Bernardino/San Gabriel subregion. Precipitation amounts (inches) are for 12 hours ending 1800 UTC 01 March 1991.

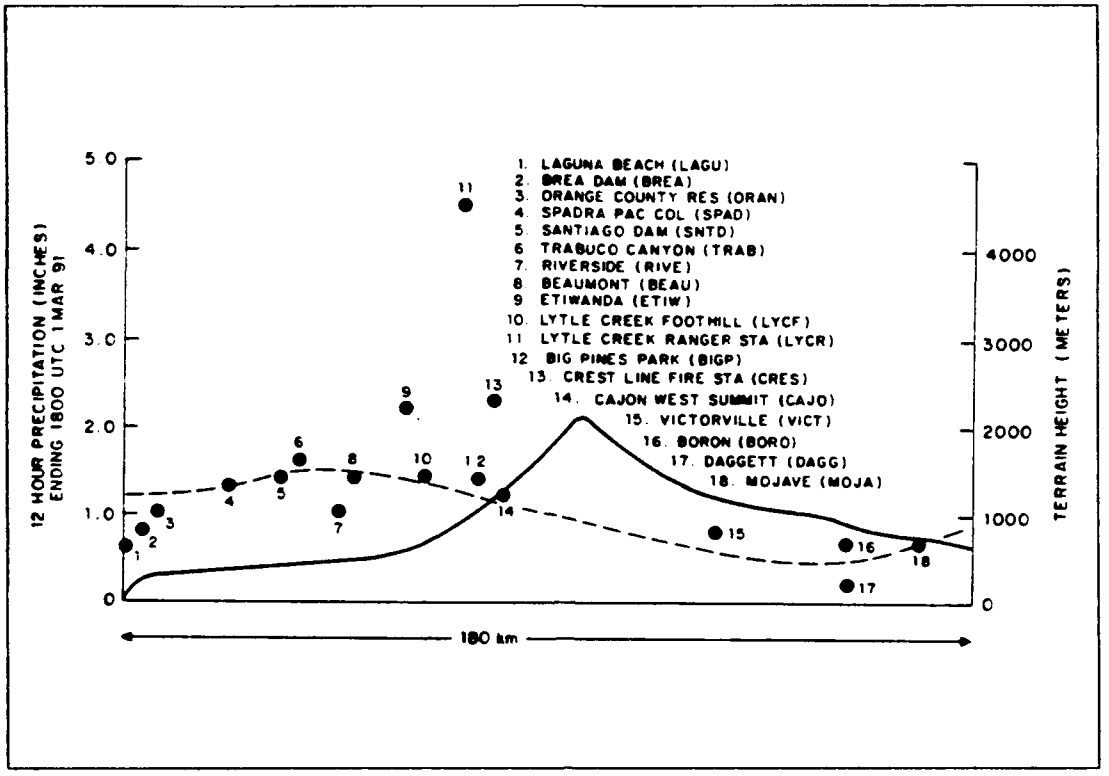

Figure 21. Topography (solid line, meters), *wqf* precipitation (dashed, inches), and observed precipitation (points, inches) for San Bernardino/San Gabriel subregion (12 hour period ending 1800 UTC 01 March 1991).

It should be mentioned that the significant rain events in both this subregion and the Santa Barbara subregion which follows ended by 1800 UTC 02 March 1991. As a result, the conditions which lead to deterioration of correlation values late in the period were not observed in these regions.

b. Santa Barbara

The Santa Barbara subregion (Figure 22) is characterized by particularly good *wqf*/precipitation correlation (Figure [illegible] ranging from

-0.52 to -0.85 for the different analysis times. Note that correlation during the post-frontal convective period of 1200 UTC 28 February 1991 - 0000 UTC 01 March 1991 shows less deterioration in this region than in the state-wide case (-0.52 vs. -0.22). Similar to the previous subregion, lee stations (NE) are represented highly accurately, with the majority of the variance seen in the upslope regions (SW). Again, subgrid-scale topography likely produces large variations over small distances.

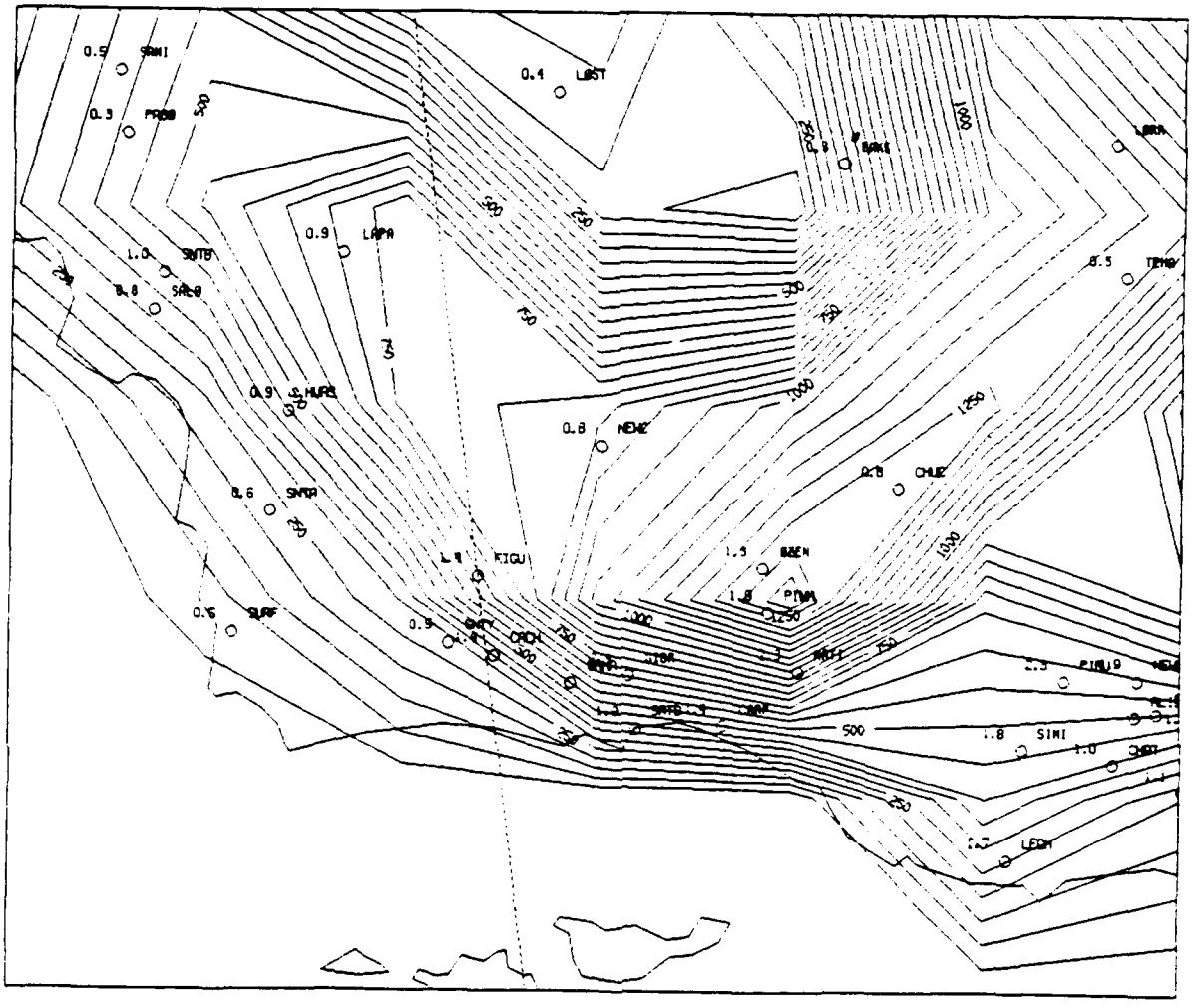

Figure 22. Topography (meters) and station names for Santa Barbara subregion. Precipitation amounts (inches) are for 12 hours ending 1800 UTC 01 March 1991.

A good example of an error caused by insufficient resolution of the topography is evident at time 0000 UTC 28 February 1991. Figure 24 shows the *wqf* maximum to be "transposed" to the southeast from the observed maximum, therefore limiting any correlation in this location. [illegible] topography in this

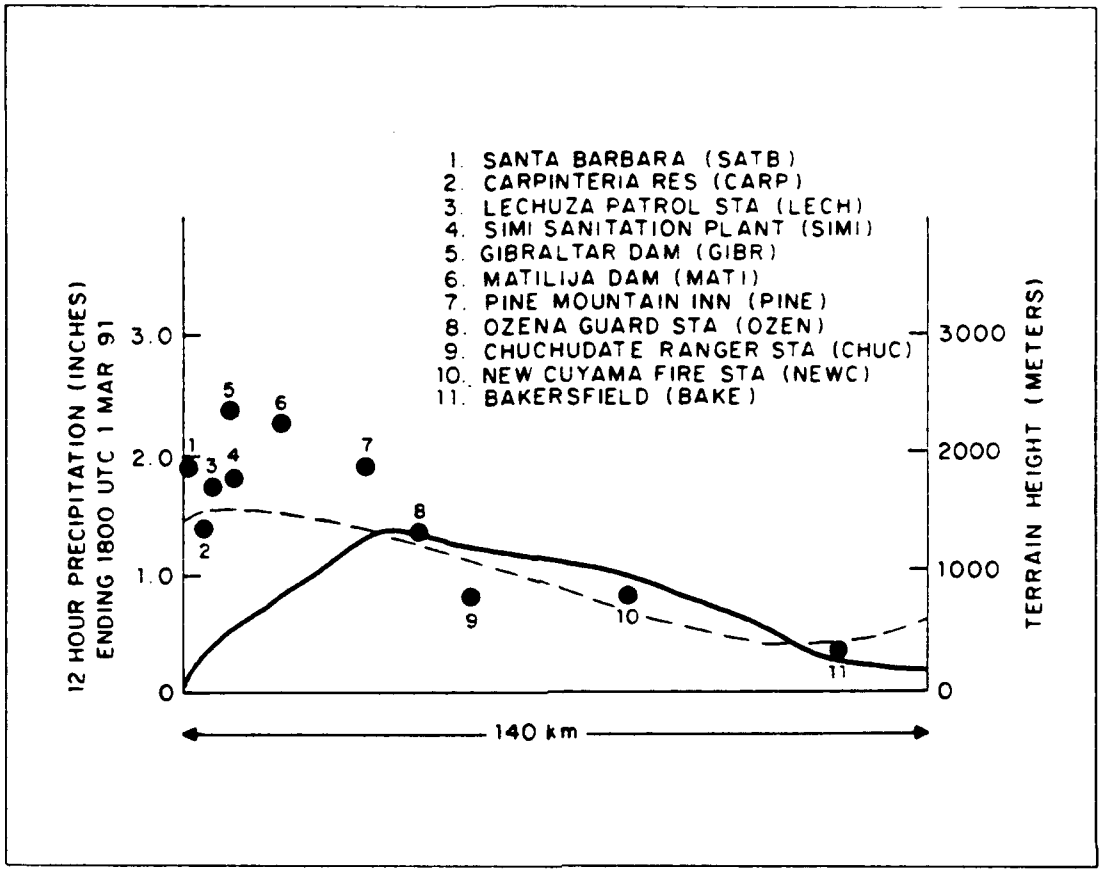

Figure 23. Topography (solid line, meters), *wqf* precipitation (dashed, inches), and observed precipitation (points, inches) for Santa Barbara subregion (12 hour period ending 1800 UTC 01 March 1991.

region (not shown) depicts a narrow northeast trending ridge in the vicinity of Thousand Oaks (station LECH), northwest of which is the Ventura Valley (station SIMI). This topography is represented as a continuous slope at 40 km resolution, however. As such, the strongest orographically forced component of *wqf* is located over the Ventura Valley (near SIMI), whereas in reality this forcing maximum is located between the Ventura Valley and Pine Mountain (station PINM). As the southeasterly winds become more southerly after this time, *wqf* and observed precipitation [illegible] and much more

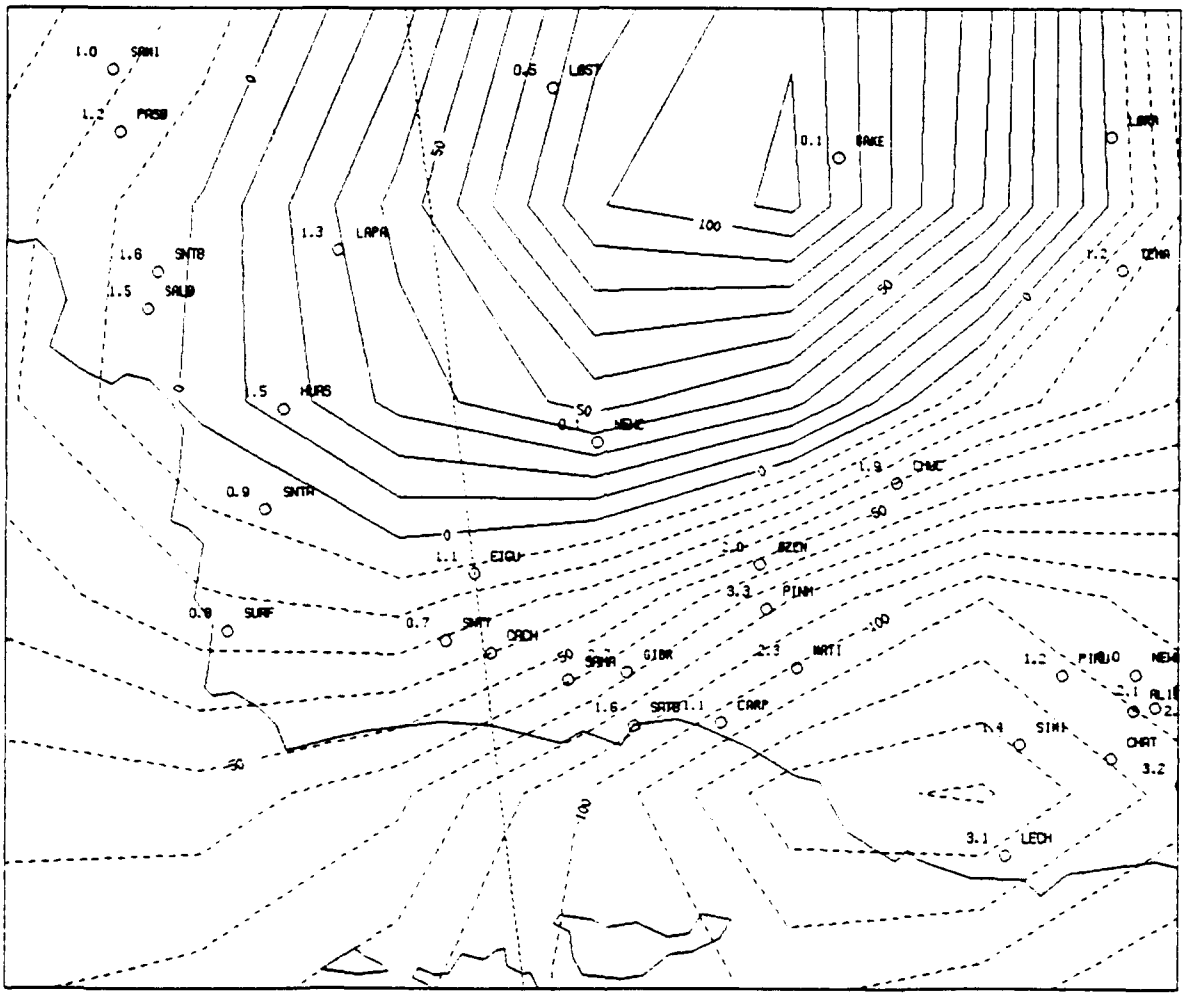

Figure 24. *Wqf* and observing stations with 12 hour precipitation totals ending 0600 UTC 28 February 1991 (inches) for the Santa Barbara subregion .

favorably, as the large-scale winds interact with topography that is better represented at the 40 km resolution.

Overestimation of precipitation at the coast (Figure 23, stations 1-5) does not seem to be as prevalent in this region. The [illegible] of the extreme slope at the land-ocean margin. Specifically, although smoothing of the topographic u-

field still produces upward orographic forcing well into oceanic regions, the rapid increase in elevation onshore produces orographically enhanced observed precipitation amounts even near the ocean. Moreover, the apparent high coastal correlation is more likely a coincidence as opposed to an increase in skill over, for example, the San Bernardino region. As with the previous sub-region, no significant precipitation was observed after 1800 UTC 02 March 1991.

c. Southern Sierra Nevada

The most notable feature seen in this region (Figure 25), commonly known as the High Sierra, is the lack of observations. Still we can make at least one important observation:

- *Wqf* generally overestimates precipitation for these inland locations.

This trend is evident throughout the study period and is represented in Figure 26. We can generally note that *wqf* responsible for a specific rain amount along the coast (i.e., Santa Barbara) represents a somewhat lesser amount at more inland locations. This feature is almost certainly a function of the available moisture, such that inland locations require a greater *wqf* to maintain saturation than is required near the coast. No effort is made to quantify this relationship, however it must be considered when using *wqf* based on inter-regional statistics (similar to adjusting Model Output Statistic (MOS) precipitation forecasts for a specific location).

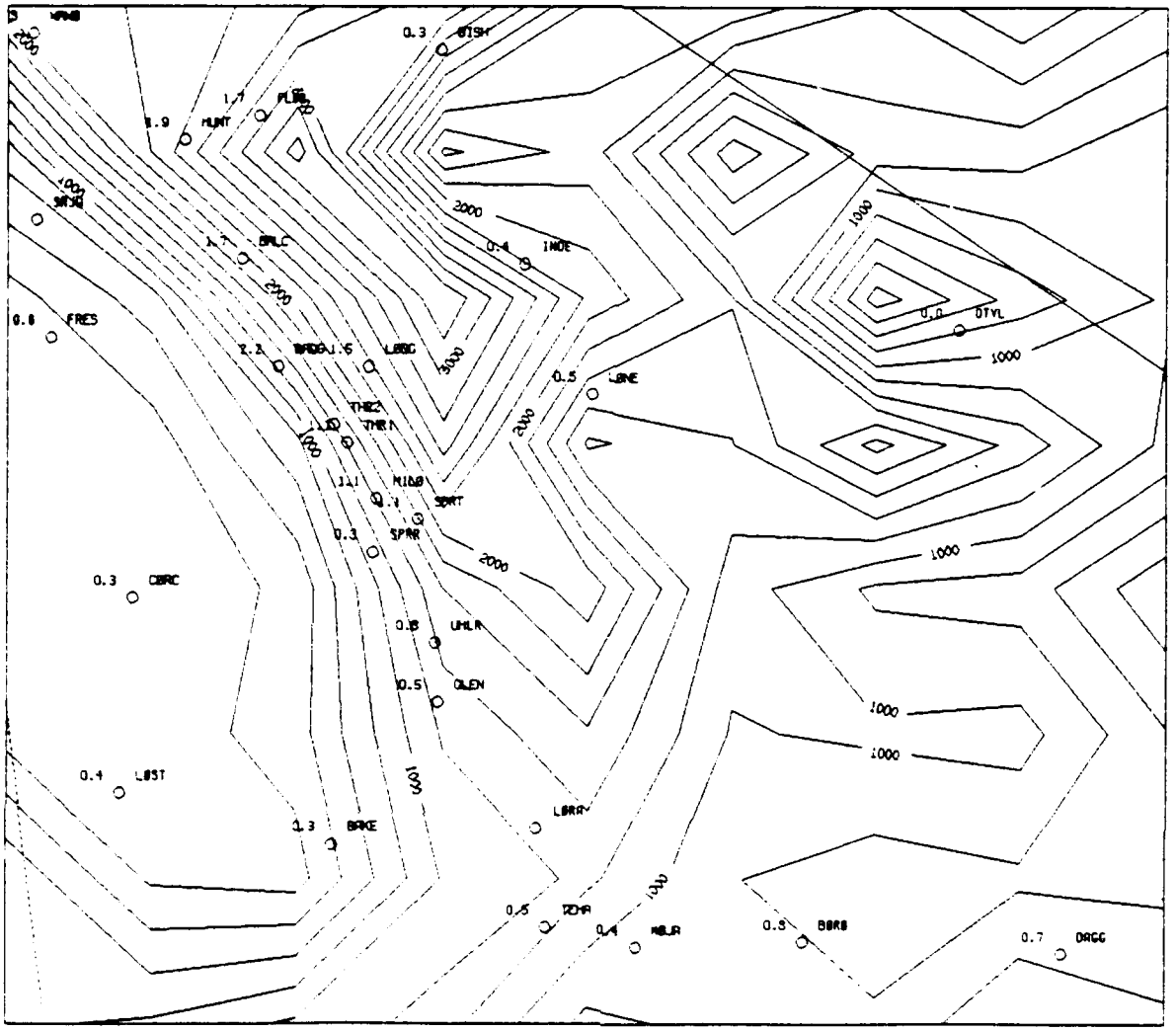

Figure 25. Topography (meters) and station names for Southern Sierra Nevada subregion with 12 hour precipitation totals (inches) ending 1800 UTC 01 March 1991.

Note that Figure 26 shows *wqf* and observed precipitation both before and after 1200 UTC 02 March 1991 with correlations of 0.75 and 0.70 respectively. Though in the latter, a large cluster of overforecasts, non-

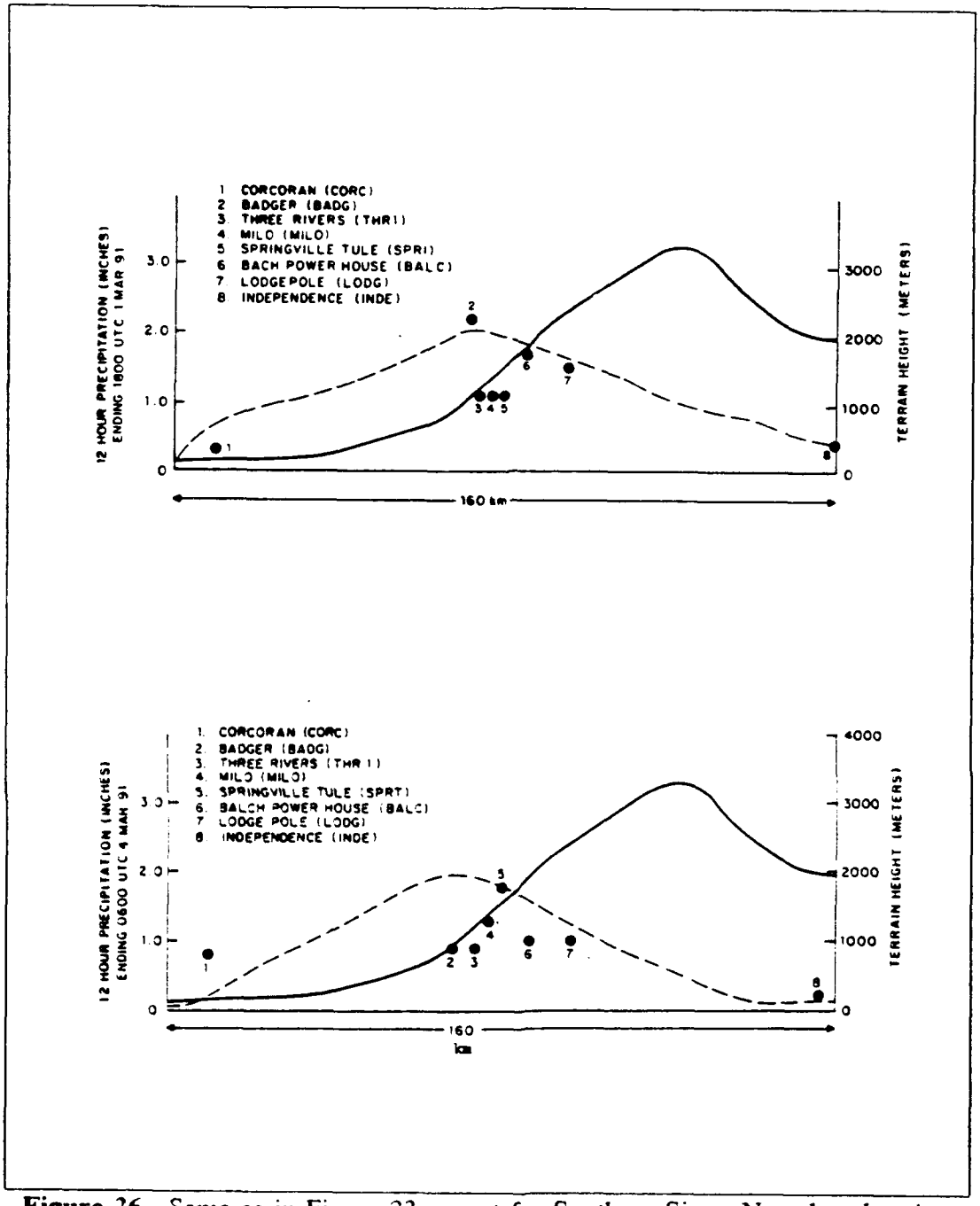

Figure 26. Same as in Figure 23 except for Southern Sierra Nevada subregion (12 hour period ending 1800 UTC 01 March 1991, top, and 0600 UTC 04 March 1991, bottom).

orographic effects are more evident, especially considering the rough equivalency of precipitation totals at the San Joaquin Valley station Corcoran (CORC) and amounts recorded higher in the Sierra. The low slope value (-0.004) of the linear regression supports this assignment.

d. Northern Sierra Nevada

This subregion (Figure 27) depicts the gradually sloping region of the Sierra Nevada between Sacramento and the Lake Tahoe basin. The chosen cross-section (Figure 28) coincides roughly with the American River drainage, which is represented particularly well by the 40 km topographic resolution. As a result, we see very good *wqf*/precipitation correlation in this sub-region prior to 1200 UTC 02 March 1991, with correlation coefficients between -0.70 and -0.80. As before, we note the overestimation of precipitation in the Sacramento valley (WHEA), as well as a general tendency to underestimate precipitation (slope values average -0.006 in this subregion). The generally good fit seen in the first period at the summit and lee stations of Soda Springs (SODA) and Truckee (TRUC) respectively represent the ability of this technique to account for lee "spillover", due to the statistical correlation producing a positive y-intercept.

Perhaps the best example of subgrid-scale processes affecting the distribution of precipitation is seen at time 1200 UTC 04 March 1991 (Figure 27). Note the extraordinarily high precipitation observations over Donner Summit, including Truckee, as compared to precipitation estimated by *wqf* (regional correlation coefficient and slope values are -0.10 and 0.000 respectively). This analysis is not resolving the wind and moisture field anomalies responsible for the distribution. This

example brings into question *wqf*'s level of usefulness given this type of synoptic situation.

Of particular note concerning this region is the ability to compare results obtained here to those obtained over a similar region by Colton's (1976) 4.3 km model. Though Colton's (1976) use of an hourly precipitation rate prohibits direct comparison to the 12 hour rate presented here, we can make some qualitative assessments. Other than Colton (1976) showing considerably greater detail within the upslope region, including the secondary maximum produced by Mt. Rose rising to the east of Lake Tahoe, *wqf* produces a similar enhancement pattern, prior to 1200 UTC 02 March 1991, in terms of the location of maximum as well as the intensity. Of further note is that even at the 4.3 km grid scale, Colton's (1976) calculations at lee stations generally underestimate precipitation, even with a "spillover" term included. However, Colton's (1976) fine mesh resolution allows a better representation of convective forcing. In these types of situations, *wqf* is far inferior to Colton's (1976) model.

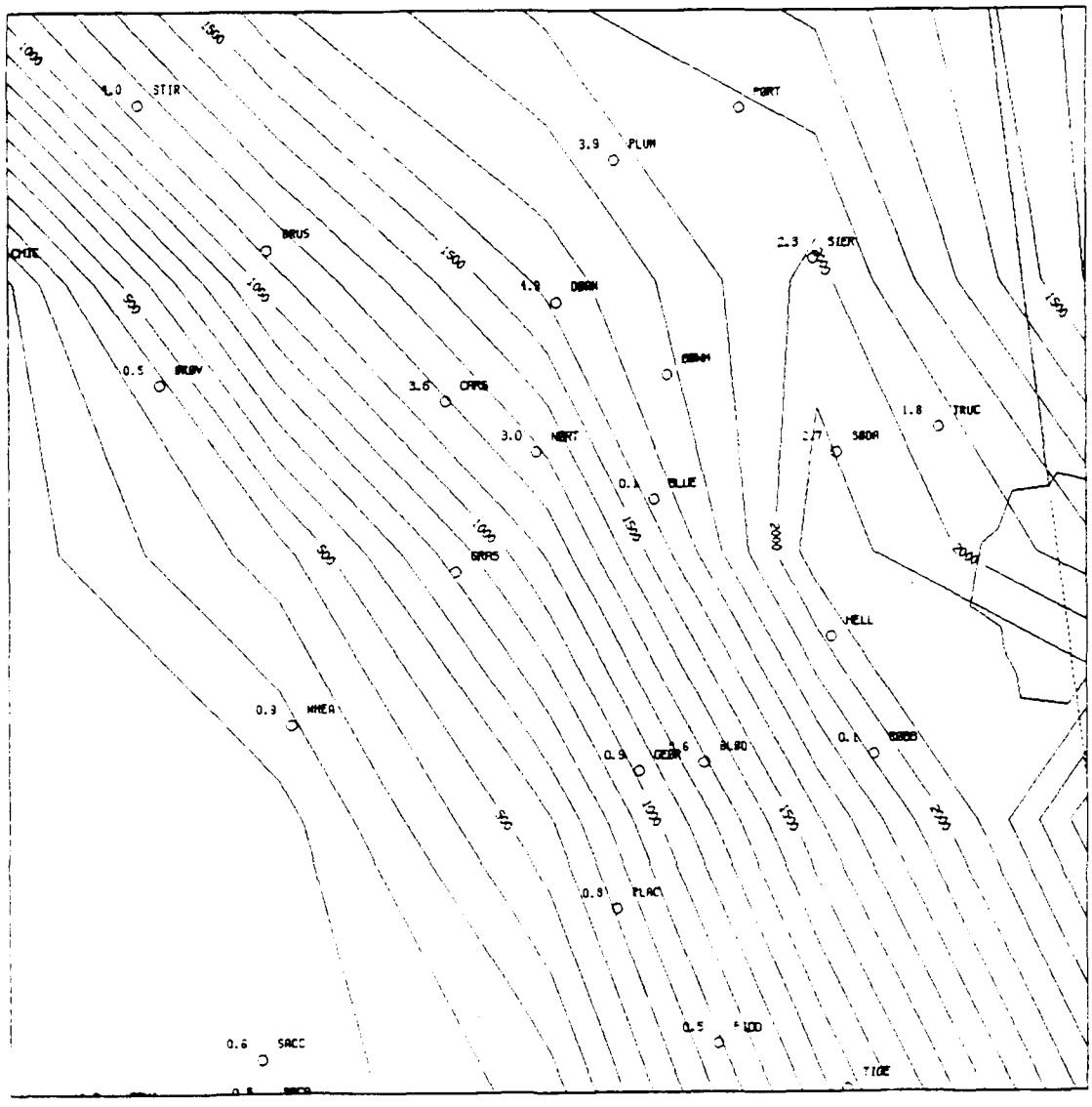

Figure 27. Topography (meters) and station names for Northern Sierra Nevada subregion with 12 hour precipitation totals (inches) ending 1800 UTC 04 March 1991.

c. Shasta/Siskiyou

The final sub-region (Figure 29) contains not only the most complicated topography, but also was subject to the [illegible] to precipitation. Figure 30 shows representative wind/precipitation plots before and after 1200 UTC

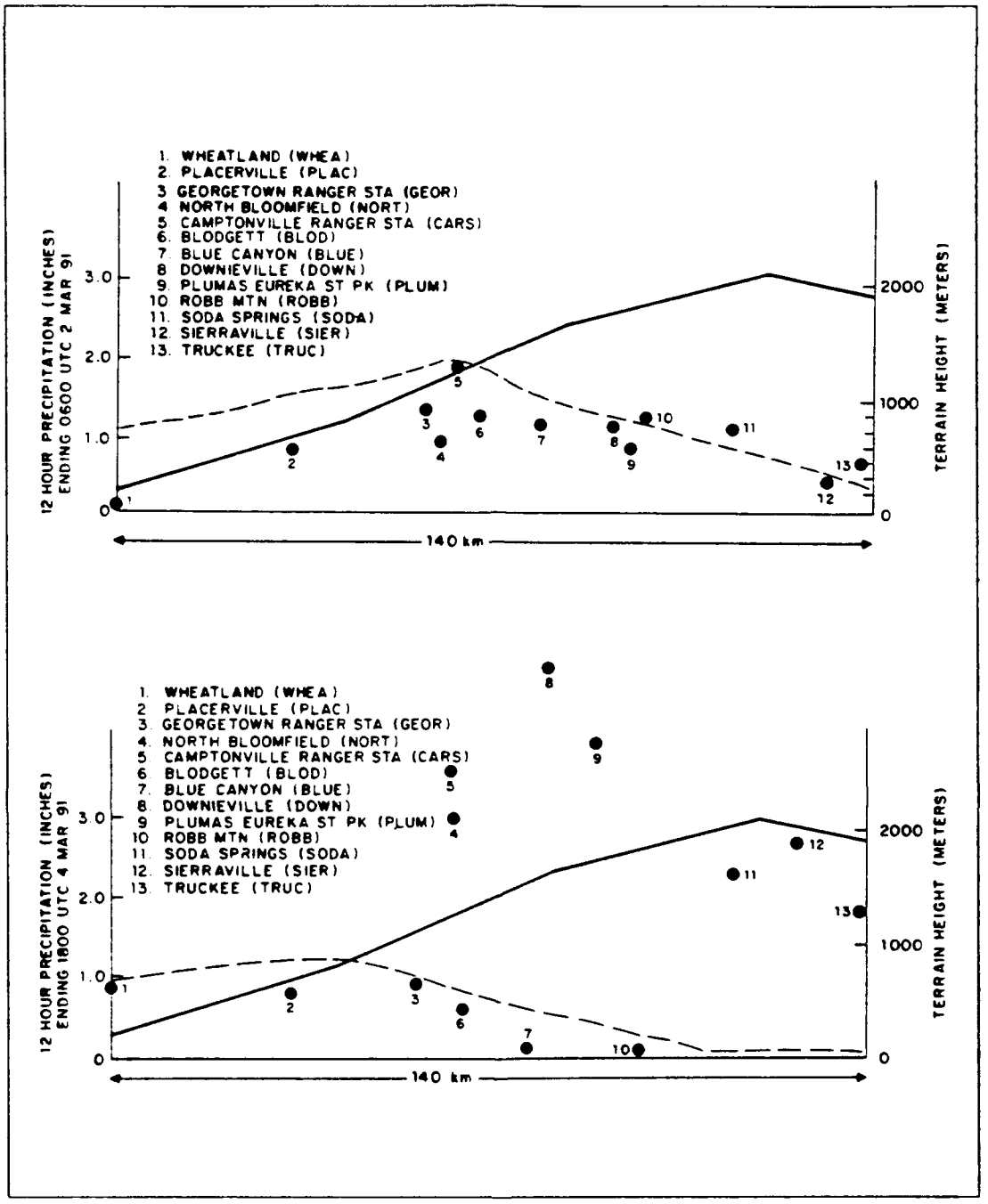

Figure 28. Same as in Figure 23 except for Northern Sierra Nevada subregion (12 hour accumulations ending 0600 UTC 02 March 1991 , top, and 1800 UTC 04 March 1991, bottom).

02 March 1991 with corresponding correlation coefficients of -0.68 and -0.46 respectively. Also, slope values for this subregion average -0.012, which, being relatively high, is consistent with its more coastal location. Despite the obvious smoothing of topographic features at this resolution, the overall *wqf* representation of precipitation is quite encouraging, in particular the secondary maximum seen between Happy Camp (HAPP) and Elk Valley (ELKV). Even more interesting is the less obvious loss of correlation late in the period. This may be due to this subregion's northernmost location. Here, synoptically derived subsidence is less than that at more southern locations at this time, allowing *wqf* to "create" upward motion by offsetting the synoptic-scale subsidence. Clearly, the improved correlation is only coincidental since convective processes are not accounted for in any region. Another possibility is more consistent forcing. The proximity of this subregion to the surface low pressure systems late in the period may have resulted in a more consistent low-level southerly flow. In this situation, though convection is still unaccounted for, the synoptic- scale winds are probably acceptable representations of the low-level flow in this subregion. This, combined with the strong tendency for the north end of the Sacramento Valley to channel winds with a southerly component may have allowed *wqf* to reach a level at least of the same order of magnitude as the convective forcing. As such, this period's correlation is likely more an effect of the particular local situation interacting with the synoptic scale, rather than *wqf* being more accurate in this subregion

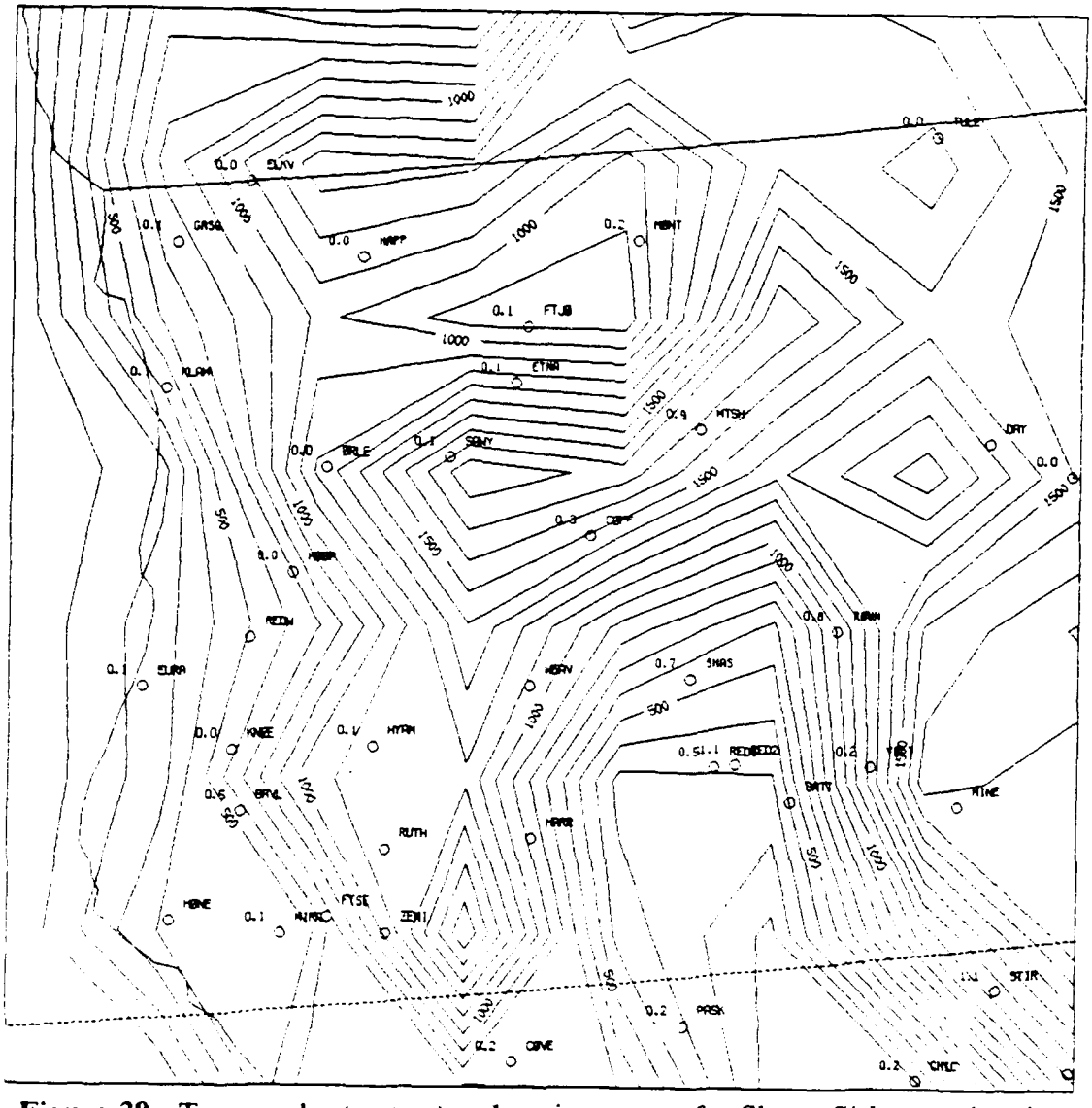

Figure 29. Topography (meters) and station names for Shasta-Siskyou subregion, with 12 hour precipitation totals (inches) ending 1800 UTC 01 March 1991.

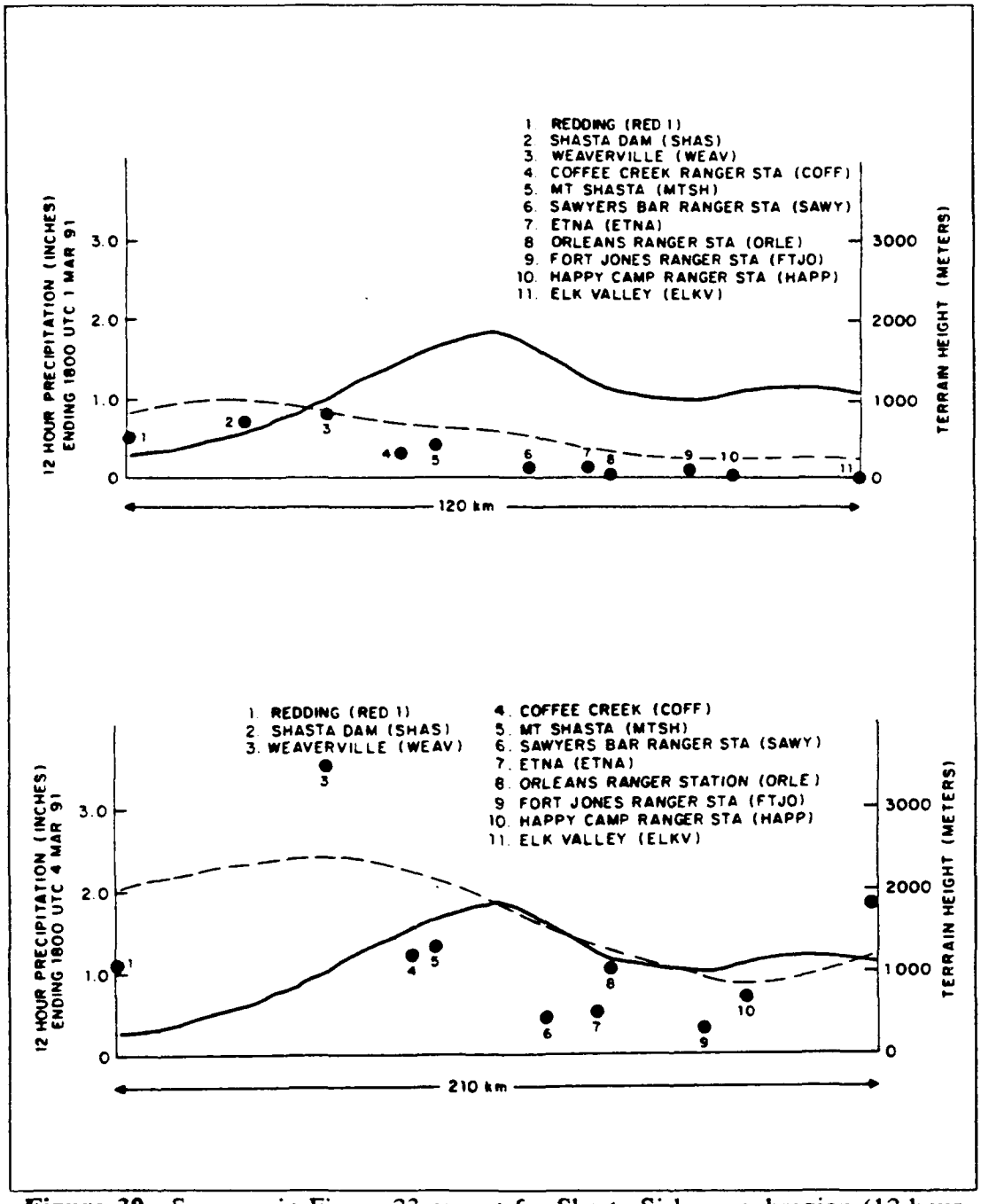

Figure 30. Same as in Figure 23 except for Shasta-Siskyou subregion (12 hour accumulations ending 1800 UTC 01 March 1991, top, and 1800 UTC 04 March 1991, bottom).

f. Non-mountainous Regions

Though this study is aimed at representing mesoscale precipitation within mountainous regions, it is also hoped that including the effects of local topography will improve distribution in low lying regions, or regions in which topography is sub-grid scale such as the Santa Cruz Mountains (Figure 31). Without going into great detail, we can qualitatively assess the success of *wqf* as weaker where topography is not as well defined. As before, regions of less dramatic topography are most susceptible to sub-synoptic processes dominating the local distribution of precipitation. This is especially evident when surface forcing is not represented well by the synoptic analysis (i.e. upper level features and convection).

As far as mountainous regions which are poorly represented at 40 km resolution, there is sufficient evidence to suggest improving topographic resolution in order to identify *wqf* forcing in these regions. Again we refer to the precipitation distribution within the Santa Cruz mountains (Figure 32). Present resolution does not see the steep, narrow nature of this range, but observations support strong local orographic influence. Increasing topographic resolution may provide sufficiently large quantities of *wqf* to "survive" the smoothing process realizing that this representation will only be of use if the synoptic analysis is at least close to reality, which is certainly far from guaranteed.

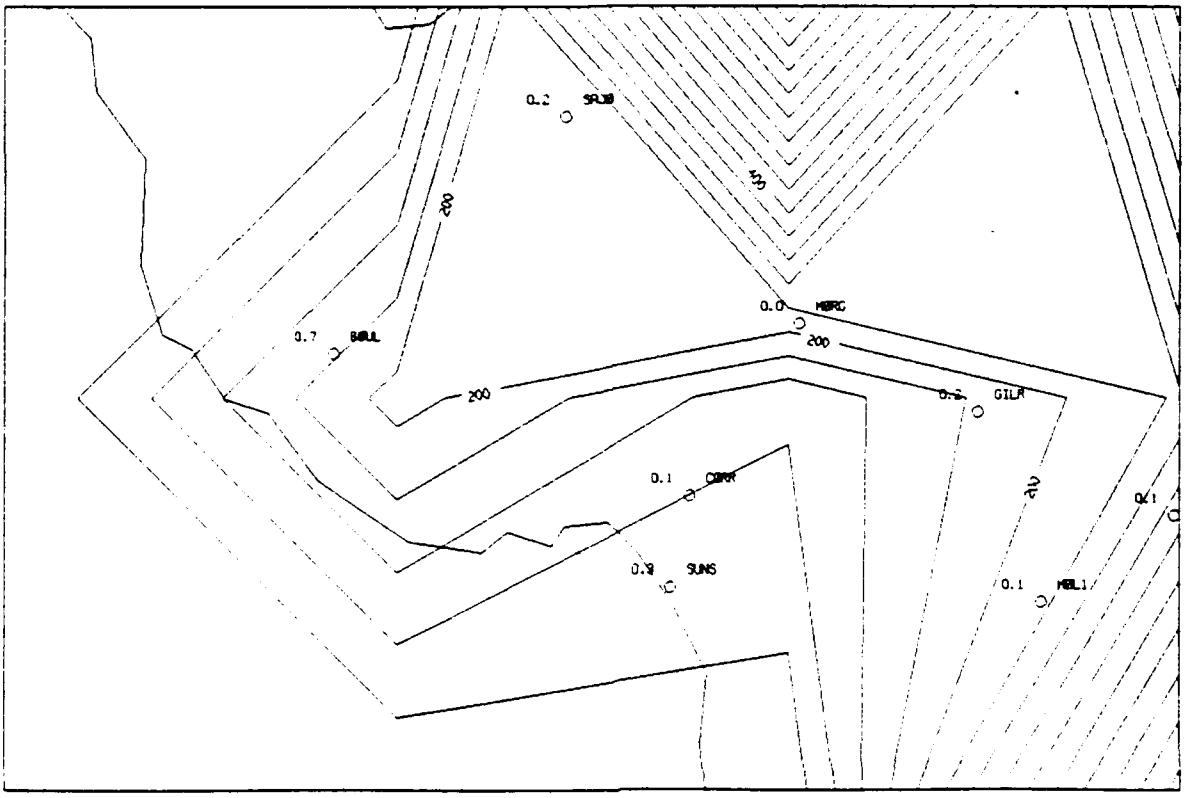

Figure 31. Topography (meters) and station names in the vicinity of the Santa Cruz Mountains with 12 hour precipitation totals (inches) ending 1800 UTC 28 February 1991.

3. Comparison to NGM Precipitation Forecasts

Earlier we established the rough equivalency of the NGM precipitation forecast with the term used here to represent synoptic-scale forcing, *w0f*. We have seen examples of the improvement the topographic forcing term has on the *w0f*, field in representing observed precipitation during the first period. This is essentially the same level of improvement *wqf* will likely [illegible] for the NGM convective parameter (this parameter will be [illegible] built

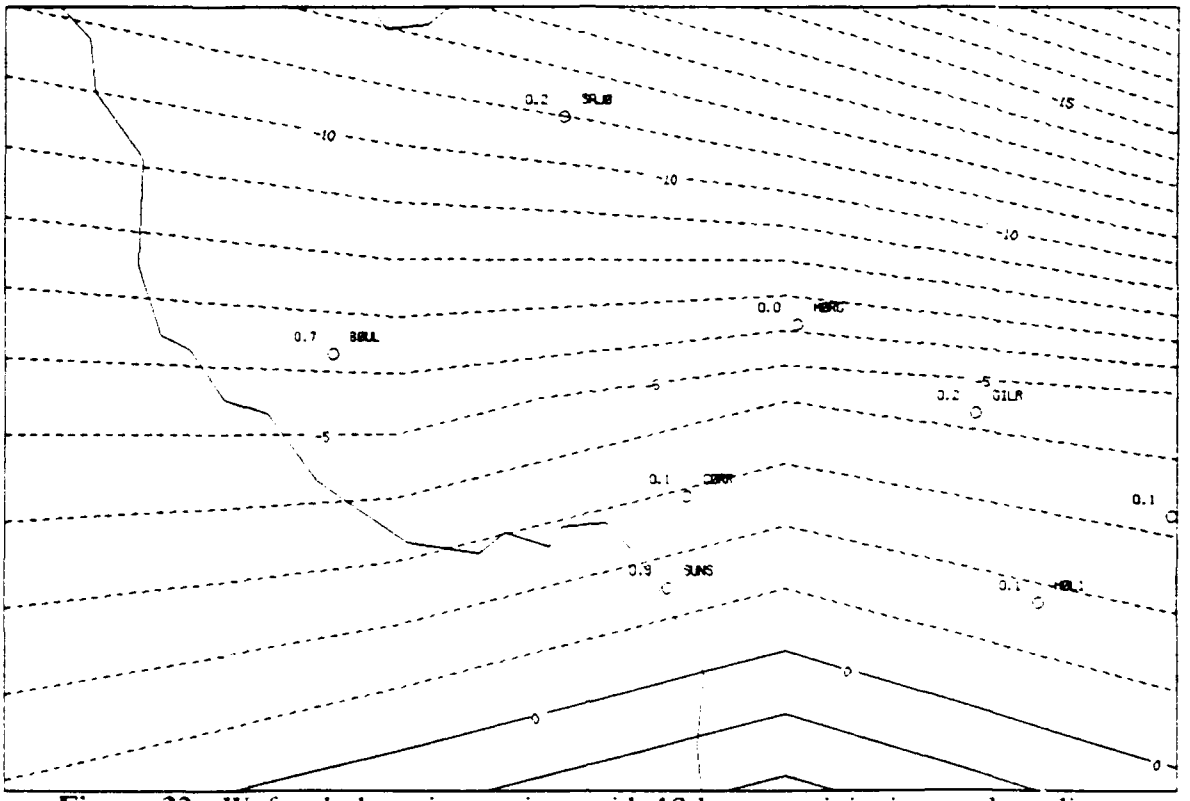

Figure 32. *Wqf* and observing stations with 12 hour precipitation totals ending 1800 28 February 1991 (inches) in vicinity of Santa Cruz Mountains.

into *wqf*). Note that while the NGM and *w0f* are able to define general precipitation areas reasonably well, there is virtually no structure other than that associated with the synoptic-scale forcing maxima (usually coincident with 700 mb vertical velocity), and therefore weak correlation with observations.

Late in the period, NGM represents precipitation with only slightly less overall accuracy than *wqf*. Recall that for these times, the NGM vertical velocity forecast predicted upward motion in areas which verified to be subsident. Still, its convective parameter may be accounting for some of the [illegible]

VI. CONCLUSIONS

A. APPLICATION TO FORECASTING

It is well known that precipitation amounts can vary dramatically over a small area. Inclusion of topography into fine-mesh models has shown favorable representation of this variability (Colton 1976, Collier 1975). Unfortunately, the data network needed to run these models is not generally available to the forecaster, who can only combine local knowledge with the synoptic-scale products he receives. In this thesis we have attempted to provide a quantitative estimate of mesoscale precipitation distributions over mountainous terrain, without requiring mesoscale information, other than topography. Conclusions can be summarized by the following points:

- Given that synoptically induced forcing is well represented in the analyzed or forecast fields, *wqf* can predict a substantial degree of the mesoscale precipitation distribution.
- Most of the discrepancies between *wqf* and the observations occur within upslope regions (as opposed to lee stations) due to unresolved small-scale topographic forcing.
- Correlation is greatly improved when considering well defined topographic regions.
- *Wqf* shows significant improvement over the NGM precipitation forecast fields.

Coincident with our conclusion that *wqf* is a good indicator of precipitation under well defined synoptic-scale forcing conditions, [illegible] when non-orographic and/or mesoscale processes dominate precipitation forcing.

Therefore, to be of use to the forecaster, he/she must first determine the applicability of *wqf* based on the synoptic situation. There is sufficient evidence to suggest *wqf* may be of some value even when no synoptic-scale forcing is indicated. In this case, the forecaster must weight the *wqf* field accordingly, but be aware that areas of consistently strong flow may still be represented by *wqf* precipitation maxima. As such, assuming *wqf* is produced as a forecast field, the forecaster must identify its credibility based on the following parameters:

- Presence of a well-defined thickness ridge ahead of a front.
- The potential for unstable precipitation.

If these conditions can be correctly evaluated, *wqf* will be sufficiently useful to the forecaster in predicting locally heavy precipitation to warrant its calculation by regional forecast offices.

B. RECOMMENDATIONS

The most immediate recommendation would be to incorporate actual NGM forecast fields into the *wqf* calculation. This would provide a basis for verifying the *wqf* precipitation against the actual NGM forecast precipitation amounts. Such an application will be able to more definitively evaluate *wqf* as a forecast parameter.

Secondly, there may be some benefit to computing *wqf* over even finer topographic resolution (i.e., 20 or even 10 km since the [illegible] precipitation will be prevalent regardless of the topographic resolution [illegible] resolution may

improve *wqf* representation of precipitation by pinpointing areas of maximum enhancement and by reflecting the orographic influence of steep topography with less horizontal extent. There will, however, most certainly be a point at which no increase in *wqf* accuracy is seen with increasing topographic resolution. Furthermore, objective restrictions potentially can be applied to the calculation of *wqf* in flat regions which are adjacent to significant topographic barriers. The intent here is to limit the forcing to the actual topographic slope rather than distributing it over a larger region as done by the current smoothing process.

As a final note, I wish to emphasize that no new ground has been broken here as far as our understanding of the precipitation process. I have simply adapted seeder-feeder theory of orographically enhanced precipitation to a format which only requires synoptic scale information. Though the results are far from ideal, I think the technique exhibited sufficient success to warrant its consideration by the forecaster.

LIST OF REFERENCES

Anderson,T., and S. Nilsson, 1990: Topographically Induced Convective Snowbands over the Baltic Sea and their Precipitation Distribution. *Wea. Forecasting*,5,299-312.

Bader, M.J., and W.t. Roach, 1977: Orographic rainfall in warm sectors of depressions.*Quart. J. R. Met. Soc.*,**103**,269-280.

Bergeron, T.,1965: On the low-level redistribution of atmospheric water caused by orography. *Proc. Int. Conf. Cloud Physics. Tokyo*, 1965, 96-100.

Browning, F.F. Hill and C.W. Pardoe, 1974: Structure and mechanism of precipitation and the effect of orography in a wintertime warm sector. *Quart. J. R. Met. Soc.*,**100**,309-330.

Browning, K.A., C.W. Pardoe and F.F. Hill, 1975: The nature of orographic rain at wintertime cold fronts. *Quart. J. R. Met. Soc.*,**101**,333-352.

Carruthers, D.J., and T.W. Choularton, 1983: A model of the feeder-seeder mechanism of orographic rain including stratification and wind-drift effects. *Quart. J. R. Met. Soc.*,**109**,575-588.

Collier,C.G.,1975: A representation of the effects of topography on surface rainfall within moving baroclinic disturbances. *Quart. J. R. Met. Soc.*,**101**,407-422.

Colton, D.E.,1976: Numerical Simulation of the Orographically Induced Precipitation Distribution for use in Hydrologic Analysis. *J. Appl. Meteor.*,**15**,1241-1251.

Danard,M.,1977: A simple model for mesoscale effects of topography on surface winds. *Mon. Wea. Rev.*,**105**,572-581.

Hill, F.F., K.A. Browning, and M. J. Bader, 1981: Radar and rain gauge observations of orographic rain over south Wales. *Quart. J. R. Met. Soc.*,**107**,643-670.

Kanamitsu,M., 1989: Description of the Global Data Assimilation and Forecast System. *Wea. Forecasting*,**4**,335-342.

NOAA, 1991: Hourly Precipitation Data for California, February Vol. 41 No. 2

NOAA, 1991: Hourly Precipitation Data for [illegible]

Raddatz, R. L., M. L. Khandekar, 1979: Upslope Enhanced Extreme Rainfall Events over the Canadian Western Plains: A Mesoscale Numerical Simulation. *Mon. Wea. Rev.*,**107**,650-660.

Sawyer,J.S., 1959: The introduction of the effects of topography into methods of numerical forecasting. *Quart. J. Roy. Meteor. Soc.*,**85**,31-43.

Storebo, P. B., 1976: Small scale topographical influences on precipitation. *Tellus*, **28**, 45-59.

Stow, D., S. Bradley, and W. Gray, 1991: A Preliminary Investigation of Orographic Rainfall Enhancement over Low Hills near Auckland New Zealand. *J. Met. Soc.* Japan,**69**,489-495.

BIBLIOGRAPHY

Holton, J. R., An Introduction to Dynamical Meteorology, Academic Press, Inc.,1979.

INITIAL DISTRIBUTION LIST

		No. Copies
1.	Defense Technical Information Center Cameron Station Alexandria, VA 22304-6145	2
2.	Library, Code 52 Naval Postgraduate School Monterey, CA 93943-5002	2
3.	Chairman (Code MR/HY) Department of Meteorology Naval Postgraduate School Monterey, CA 93943-5000	1
4.	Professor Wendell A. Nuss (Code MR/Nu) Department of Meteorology Naval Postgraduate School Monterey, CA 93943-5000	2
5.	Professor Patricia M. Pauley (Code MR/Pa) Department of Meteorology Naval Postgraduate School Monterey, CA 93943-5000	1
6.	Lt. Michael D. Angove USS Belleau Wood LHA-3 FPO AP 96623-1610	1
7.	Commander Naval Oceanography Command Stennis Space Center MS 39529-5000	1
8.	Commanding Officer Fleet Numerical Oceanography Center Monterey, CA 93943-5005	1

9. Commanding Officer — 1
Naval Oceanographic and
Atmospheric Research Laboratory
Stennis Space Center
MS 39529-5004

10. Director — 1
Naval Oceanographic and
Atmospheric Research Laboratory
Monterey, CA 93943-5006

11. Chief of Naval Research — 1
800 North Quincy Street
Arlington, VA 22217

12. Office of Naval Research — 1
Naval Ocean and Research and
Development Activity
800 N. Quincy Street
Arlington, VA 22217